vS30, κ, regional attenuation and Mw from accelerograms: application to magnitude 3-5 French earthquakes

Stéphane Drouet, Fabrice Cotton, Philippe Guéguen

Geophysical Journal International

Geophys. J. Int. (2010) **182,** 880–898 doi: 10.1111/j.1365-246X.2010.04626.x

v_{S30}, κ, regional attenuation and $M_{\rm w}$ from accelerograms: application to magnitude 3–5 French earthquakes

Stéphane Drouet, Fabrice Cotton and Philippe Guéguen

LGIT, CNRS, LCPC, Université Joseph Fourier, BP 53, 38041 *Grenoble Cedex* 9, *France. E-mail: stephane.drouet@obs.ujf-grenoble.fr*

Accepted 2010 April 13. Received 2010 April 7; in original form 2009 November 5

SUMMARY

We investigate recordings from weak to moderate earthquakes, with magnitudes ranging between about 3 and 5, recorded by the French Accelerometric Network. *S*-wave spectra are modelled as a product of source, propagation and site terms. Inverting large data sets of multiple earthquakes recorded at multiple stations allows us to separate the three contributions. Source parameters such as moment magnitude, corner frequency and stress drop are estimated for each earthquake. We provide the first complete and homogeneous catalogue of moment magnitudes for France, for the events with magnitude greater than 3 that occurred between 1996 and 2006. Stress drops are found to be regionally dependent as well as magnitude dependent, and range from about 0.1 MPa (1 bar) to about 30 MPa (300 bars). The attenuation parameters show that, in France on a nationwide scale, variations of attenuation properties do exist. Site transfer functions are also computed, giving the level of amplification at different frequencies with respect to the response of a generic rock site (characterized by an average 30 m *S*-wave velocity, v_{s30}, of 2000 m s^{-1}). From these site terms, we compute the high-frequency fall-off parameter κ [modelled as $\exp(-\pi\kappa f)$, with f the frequency] for 76 stations. We also determine rock stations v_{s30} and we show the κ–v_{s30} relationship for 21 rock stations.

Key words: Fourier analysis; Earthquake ground motions; Earthquake source observations; Body waves; Seismic attenuation; Site effects.

GJI Seismology

1 INTRODUCTION

Ground-motion prediction equations are usually obtained from regression analysis of strong ground-motion data (see Douglas 2003, for a review). In areas of moderate-to-low seismic activity, it is common to have few recorded strong ground motions. As a consequence, the prediction of the expected ground motion for hypothetical future earthquakes is often performed through stochastic simulations (Boore 2003), or by selecting and adjusting empirical models from other regions (e.g. Cotton *et al.* 2006). In this context, Campbell's hybrid empirical approach (Campbell 2003; Campbell & Bozorgnia 2004) provides a methodological framework to adapt ground-motion prediction equations to arbitrary target regions, by using response spectral host-to-target-region conversion functions. The purpose of those transfer functions is the removal of the effects of the host region characteristics in terms of attenuation, geometrical spreading, average stress drop, site effect, etc., and their replacement by the equivalent effects for the target region. This can improve the overall usefulness of a particular empirical model for a target region of interest. A small number of observed ground-motion records can then help to rank the adjusted ground motion models in a systematic and comprehensible way (e.g. Scherbaum *et al.* 2004).

Several issues related to source, path and local site effects must be resolved before one can properly select, adjust and rank allogeneous models in low-seismicity areas.

(1) Recent ground-motion prediction equations use the moment magnitude scale. Compatibility must therefore be achieved between this moment magnitude scale and the magnitude scale describing the earthquakes used for ground-motion prediction in Probabilistic Seismic Hazard Analysis (PSHA). However, there is currently no systematic moment magnitude ($M_{\rm w}$) determination in many countries, and generally only local magnitudes ($M_{\rm L}$) are estimated homogeneously since the 1960s. For example, calibration of the relationship between $M_{\rm w}$ and $M_{\rm L}$ is currently an issue for French PSHA analysis: the local magnitudes estimated in France are known to be higher than the $M_{\rm L}$ of neighbouring countries (Braunmiller *et al.* 2005); and large discrepancies exist between the $M_{\rm w}$ and $M_{\rm L}$ estimated from punctual studies of specific earthquakes (Dufumier 2002).

(2) No consensus exists on the regional dependence of ground motion (Douglas 2007). Differences between recent ground-motion prediction equations derived in the United States and in Europe are slight (Campbell & Bozorgnia 2006; Stafford *et al.* 2008). However, intensity studies have long since shown a regional dependence of the attenuation of intensity with distance (e.g. Bakun & Scotti 2006). Recent studies of regional weak motions (e.g. Bay *et al.* 2003; Akinci *et al.* 2006; Malagnini *et al.* 2007; Drouet *et al.* 2008a; Edwards *et al.* 2008; Atkinson & Morrison 2009) confirm that clear regional particularities exist in terms of attenuation and/or stress drop. There is then a need to analyse the regional variation of ground

motion and the scaling of both geometrical spreading and stress drops with magnitude (e.g. Bay *et al.* 2005; Cotton *et al.* 2008).

(3) The average 30 m shear wave velocity (v_{s30}) is widely used as the number characterizing the site effect in the context of ground-motion prediction equations. There is then a need to characterize the v_{s30} at the stations of the target region. This value is usually determined from direct borehole or geophysical measurements. However, the associated cost of these measurements is high (some thousands or tens of thousands of euros depending on the method used), and as such there is a real interest to develop cheaper alternative methods. As most PSHA studies are performed for rock conditions, it is particularly crucial to obtain these measurements for rock stations.

(4) In addition to v_{s30}, one other site parameter, the high-frequency decay (κ or $f_{\max}$), has a primary influence on the adjustments required (Cotton *et al.* 2006). That decay has been observed and modelled through two different ways: the κ model [Anderson & Hough 1984, $\exp(-\pi\kappa f)$]; and the $f_{\max}$ model {Hanks 1982; Boore 2003, $[(1+(f/f_{\max})^8]^{-1/2}$}. Those studies demonstrate that the high-frequency decay is mainly a site term. A source dependency of κ has been demonstrated by Papageorgiou & Aki (1983) or Purvance & Anderson (2003) however this source component has a smaller effect than the site component. The clear dependence of κ on the site suggests a potential relationship between κ and v_{s30}. However, to our knowledge, only the Silva *et al.* (1998) and Chandler *et al.* (2006) papers investigate such a relationship.

The development and improvement of accelerometric networks provide an opportunity to analyse these issues. In Europe, several networks have recorded high-quality small-to-moderate events (http://itaca.mi.ingv.it/ItacaNet/, http://www-rap.obs.ujf-grenoble.fr/, http://www.seismo.ethz.ch/). The advantage of these weak-motion databases compared with the international strong ground-motion databases, such as the NGA (Next Generation Attenuation of ground motions) database, is the homogeneous coverage of a unique region. This allows the recovery of path and site terms. So in this study, we use data from the French Accelerometric Network (RAP, Pequegnat *et al.* 2008) to analyse source, path and site effects for three different tectonic regions (French Pyrenees, French Alps and Rhine Graben). We compute moment magnitudes and corner frequencies for 161 events and deliver a moment magnitude catalogue of French earthquakes recorded between 1996 and 2006 in these tectonic regions. Our inversion procedure also characterizes the geometric and anelastic attenuation parameters for these three tectonic regions. We finally describe the site transfer functions of 76 accelerometric stations. A new method, developed to analyse these site transfer functions, allows the determination of κ and v_{s30} at the rock stations. This new $\kappa - v_{s30}$ relationship is finally presented and discussed. Those results supersede those from our previous studies (Drouet *et al.* 2005, 2008a) as the amount of data has more than doubled and the inversion is performed for a wider frequency range (now up to 30 Hz compared to 15 Hz). Moreover, the inversion procedure has been modified to work with acceleration spectra rather than displacement spectra (reducing the processing used) and the site terms are determined relative to a quantified reference (i.e. a rock site with $v_{S30} = 2000$ m s^{-1}).

2 DATA

The French Accelerometric Network (Réseau Accélérométrique Permanent, RAP) has been operating since 1996. Today more than 100 stations cover the national French territory providing high-quality data, even for small events, which is freely available at the National Data Center RAP-NDC: http://www-rap.obs.ujf-grenoble.fr/ (Pequegnat *et al.* 2008).

On the basis of the RAP recordings, three regional data sets for France have been constructed (Fig. 1). The records of earthquakes with local magnitude greater than 3 are kept if at least three different recordings with a distance greater than 15 km are available. These are the same criteria as in a previous paper (Drouet *et al.* 2008a) however the number of analysed spectra has since more than doubled. The final data set is composed of 72 earthquakes in the Alps (Table 1), 23 in the Rhine Graben (Table 2) and 66 in the Pyrenees (Table 3). The hypocentral information comes from the French national network RéNaSS, whereas local magnitudes are given by two national agencies: RéNaSS and LDG (M_{ren} and M_{ldg}). Fig. 1 shows the locations of the three regions within France and the earthquakes, stations and paths for each region.

Each three-component recording has been visually inspected and the *P*- and *S*-wave arrival times have been picked. As in Drouet *et al.* (2008a), a 5 s time window is used to select the direct *S* waves for all the distances, and acceleration Fourier spectra are computed. The spectra are then smoothed between 0.5 and 30 Hz using a Konno–Ohmachi procedure (Konno & Ohmachi 1998). Noise spectra are similarly computed, using the pre-recorded window before the *P*-wave arrivals. The north–south and east–west components (of signal and noise) are combined, to get a single horizontal component, as follows:

$$S(H) = \sqrt{S(E)^2 + S(N)^2}. \tag{1}$$

A minimum signal-to-noise (S/N) ratio of 3 is imposed at each frequency. Consequently, some points between 0.5 and 30 Hz might be missing in some spectra. To minimize this problem, a minimum of 60 per cent of the total number of frequencies with S/N ratio above 3 must be included in a record.

3 METHOD

The *S*-wave acceleration spectrum $A_{ijk}(r_{ij}, f_k)$ can be written as the product of a source, a propagation and a station term.

$$A_{ijk}(r_{ij}, f_k) = \Omega_i(f_k)\, D_{ij}(r_{ij}, f_k)\, S_j(f_k), \tag{2}$$

where r_{ij} is the hypocentral distance from earthquake i to station j and f_k the frequency. We adopt the far-field acceleration spectrum given by Brune's model (Brune 1970, Brune 1971).

$$\Omega_i(f_k) \sim \frac{(2\pi f_k)^2\, M_{0_i}}{\left[1+\left(\frac{f_k}{f_{c_i}}\right)^2\right]}, \tag{3}$$

where M_{0_i} is the seismic moment and f_{c_i} the corner frequency of event i.

Attenuation involves anelastic decay and geometrical spreading.

$$D_{ij}(r_{ij}, f_k) = \exp\left(-\frac{\pi r_{ij} f_k}{Q(f_k) v_S}\right) \times \frac{1}{r_{ij}^{\gamma}}, \tag{4}$$

where v_S is the average *S*-wave velocity along the path and $Q(f_k) = Q_0 \times f_k^{\alpha}$ is the frequency-dependent quality factor. Note that the geometrical spreading may differ from the classical r_{ij}^{-1} form through the coefficient γ. We expect γ to be greater than 1, because downward reflections from layer interfaces (e.g. Frankel 1991) and scattering (e.g. Gagnepain-Beyneix 1987) can result in a geometrical loss of energy.

Considering the moderate magnitudes of the largest analysed events and the minimum frequency of 0.5 Hz, a minimum hypocentral distance of 15 km was required, for the far-field approximation to be valid (e.g. Aki & Richards 2002).

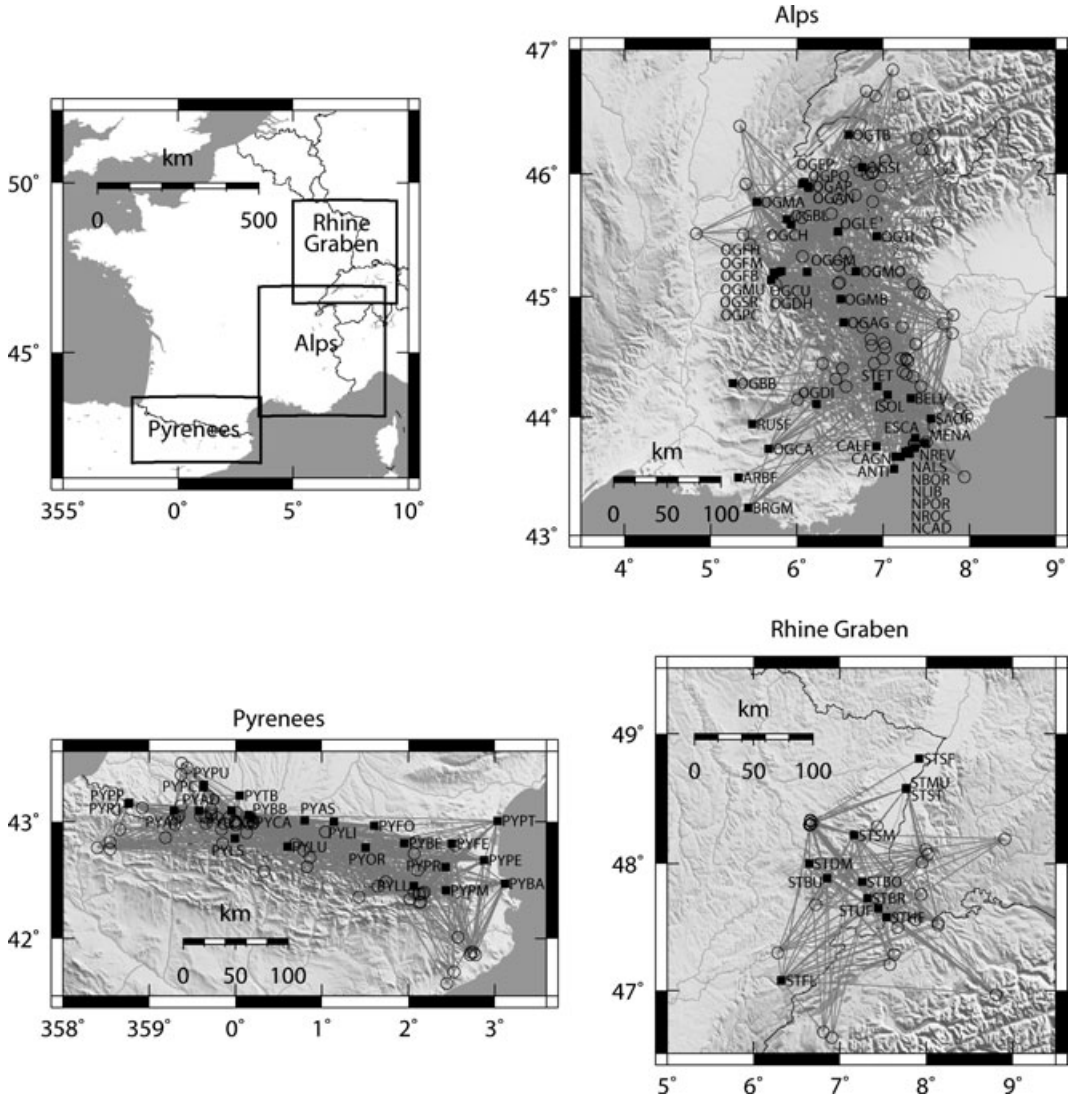

Figure 1. Maps of the earthquakes (circles), stations (squares) and paths (lines) used in this study for the three data sets: Alps, Rhine Graben and Pyrenees (see the map of France, top left frame).

$S_j(f_k)$ is the site effect at the station j. This term is equal to unity for all frequencies in the absence of site effect ('rock' site conditions). The so-called $f_{\max}$ effect (Hanks 1982) or κ effect (Anderson & Hough 1984) describes the observed strong attenuation of the high-frequencies. Although the origin of this effect is not completely understood an important contribution comes from the high intrinsic attenuation in the most superficial layers (Hanks 1982). Drouet *et al.* (2008a) used frequencies up to 15 Hz to avoid or limit the $f_{\max}$ effect. In this study, we assume that this effect is a site term (Hanks 1982) and that it will be resolved in the $S_j(f_k)$ parameter elements without using any extra parameters.

Eq. (2) may thus be rewritten as

$$y_{ijk} = m_{0_i} - \log_{10}\left[\left(\frac{(2\pi f_k)^2}{1+\left(\frac{f_k}{f_{c_i}}\right)^2}\right)\right] - \gamma \log_{10}(r_{ij}) - \frac{\pi r_{ij} f_k}{\log_e(10) Q_0 f_k^{\alpha} v_S} + s_{jk}, \quad (5)$$

where

$$y_{ijk} = \log_{10}\left[A_{ijk}(r_{ij}, f_k)\right], \quad (6)$$

$$m_{0_i} = \log_{10}\left[M_{0_i} \times \frac{2R_{\theta\phi}}{4\pi\rho\beta^3}\right], \quad (7)$$

$$s_{jk} = \log_{10}\left[S_j(f_k)\right], \quad (8)$$

with $R_{\theta\phi}$ the source radiation pattern, assumed to be constant ($R_{\theta\phi} = 0.55$ for S waves, Boore & Boatwright 1984), ρ the density, β the S-wave velocity of the medium at the source and v_S the S-wave velocity along the path (we assume $\beta = v_S = 3.5\,\mathrm{km\,s^{-1}}$ and $\rho = 2800\,\mathrm{kg\,m^{-3}}$). The factor 2 in eq. (7) accounts for the free surface reflection at the station assuming a quasi-vertical incidence. This is exact for *SH* and a reasonable approximation for quasi-vertical *SV* (Aki & Richards 2002).

Additionally, we want to compute 'absolute' site effects; thus we normalize the input spectra to a common reference accounting for crustal amplification. To do this, a generic rock velocity profile with depth associated with a v_{s30} of 2000 $\mathrm{m\,s^{-1}}$ (Boore & Joyner 1997; Cotton *et al.* 2006) is computed together with the corresponding amplification spectrum. Examples of generic amplifications computed from generic profiles with different v_{s30} values and for a *SH*-wave

Table 1. Earthquakes analysed for the Alps.

Number	Date	Hour	Latitude	Longitude	Depth (km)	M_{ldg}	M_{ren}	Number of records	Distance range (km)	M_w	f_c
1	15-05-1997	00:24:05	45.23	6.62	3	3.8	4.1	4	49/93	3.2	1.58
2	03-10-1997	15:03:35	44.32	6.45	6	3.8	4.0	4	39/101	3.3	2.86
3	31-10-1997	04:23:44	44.26	6.57	2	4.7	4.8	10	63/201	4.0	1.11
4	06-11-1997	12:39:49	44.41	6.53	2	3.6	3.7	4	79/103	3.2	2.29
5	08-11-1997	01:56:09	44.07	7.89	2	–	4.1	6	28/213	3.5	3.35
6	30-03-1998	20:49:00	46.64	7.23	10	–	3.2	3	75/165	2.8	6.27
7	11-04-1998	11:05:03	44.61	7.38	10	4.0	3.8	9	54/168	3.5	2.99
8	06-05-1998	12:02:26	44.15	6.01	10	–	3.2	4	20/118	3.0	3.01
9	13-05-1998	21:11:55	44.45	6.30	5	–	3.1	3	38/86	2.6	5.34
10	09-12-1998	22:08:16	46.20	7.45	2	3.4	3.5	5	55/136	3.1	2.19
11	11-01-1999	03:36:37	45.10	5.76	2	4.2	4.1	11	60/196	3.5	3.26
12	14-02-1999	05:57:55	46.84	7.11	2	4.7	3.8	9	70/233	4.0	1.79
13	25-04-1999	20:36:50	45.91	6.97	2	–	3.0	6	23/123	2.8	3.08
14	30-04-1999	20:59:11	44.01	7.97	2	–	3.2	4	33/89	3.1	3.31
15	10-06-1999	16:16:12	45.65	6.06	2	–	3.1	4	34/104	2.8	3.18
16	28-08-1999	15:03:15	45.26	6.48	2	–	3.3	6	17/63	3.2	2.91
17	13-09-1999	23:27:11	45.51	5.38	10	4.0	3.5	11	33/170	3.2	4.27
18	01-11-1999	17:22:35	43.78	7.36	4	–	3.3	3	27/137	2.8	3.80
19	01-04-2000	01:21:39	45.04	7.43	5	3.1	3.0	6	61/132	3.1	4.39
20	05-04-2000	08:38:22	45.52	4.84	2	3.4	3.2	6	61/161	3.0	5.77
21	31-05-2000	07:46:08	44.75	7.22	10	3.5	3.2	9	55/150	3.2	4.69
22	10-06-2000	02:44:31	44.47	7.29	5	3.5	3.2	9	37/145	3.1	4.32
23	26-06-2000	19:29:18	44.45	6.90	2	3.6	3.3	11	21/183	3.3	2.49
24	19-08-2000	08:37:26	46.10	6.68	10	4.0	3.5	8	27/126	3.4	2.41
25	19-12-2000	14:20:50	43.78	7.37	5	3.7	3.4	4	27/131	3.6	1.04
26	20-12-2000	05:45:15	43.78	7.37	5	3.2	3.0	4	27/131	3.2	1.32
27	25-01-2001	02:17:15	46.03	6.73	6	3.3	3.0	9	34/123	2.8	5.33
28	23-02-2001	22:19:42	46.11	7.03	7	3.9	3.6	10	41/144	3.3	4.21
29	25-02-2001	01:22:31	46.11	7.02	7	3.5	3.2	7	40/144	3.1	2.56
30	14-03-2001	07:09:53	43.50	7.94	7	4.1	3.8	8	48/154	3.6	3.28
31	30-05-2001	22:43:51	45.80	6.49	6	3.6	3.3	12	30/113	2.9	5.64
32	01-07-2001	19:37:20	44.58	7.03	5	3.7	3.4	12	37/178	3.3	2.75
33	09-07-2001	22:50:03	46.04	7.67	7	3.4	3.3	3	108/169	3.0	4.39
34	16-10-2001	04:18:30	45.11	6.48	6	3.4	3.1	7	16/105	3.0	2.68
35	26-01-2002	07:35:47	44.36	7.27	5	3.5	3.0	8	30/149	3.2	3.35
36	21-04-2002	17:57:17	45.61	7.63	5	3.5	3.3	4	90/165	3.1	3.16
37	06-05-2002	06:42:53	44.49	7.27	5	3.5	3.0	6	37/154	3.1	5.95
38	31-05-2002	16:50:34	46.29	7.39	5	3.6	3.5	4	106/155	3.2	3.40
39	04-02-2003	20:49:41	46.05	7.77	5	3.6	3.4	7	90/177	3.1	4.06
40	10-03-2003	13:25:06	44.85	7.81	10	3.5	3.1	7	96/175	3.0	6.74
41	29-04-2003	04:55:08	46.32	7.59	5	4.2	3.9	12	76/192	3.5	3.61
42	25-05-2003	23:03:32	45.12	6.50	5	4.0	3.6	23	16/172	3.4	1.85
43	10-06-2003	22:59:47	44.78	7.70	5	3.8	3.4	19	84/250	3.2	5.81
44	17-08-2003	22:31:51	44.65	6.86	5	3.4	3.2	6	44/195	3.1	3.07
45	01-09-2003	19:28:11	44.26	7.44	5	3.7	3.4	8	32/198	3.4	2.03
46	16-10-2003	16:23:26	44.62	7.01	5	3.4	3.1	7	41/115	3.0	4.22
47	02-12-2003	17:08:23	46.39	5.34	5	3.1	3.0	4	70/137	2.7	8.64
48	09-12-2003	18:03:07	45.33	6.07	5	3.1	3.0	11	24/65	2.8	3.07
49	20-12-2003	03:29:41	44.49	7.21	5	3.6	3.3	21	34/195	3.2	3.23
50	21-12-2003	01:35:57	44.49	7.00	5	3.5	3.1	10	27/125	3.2	2.46
51	28-01-2004	20:09:22	45.43	5.46	5	3.8	3.3	16	33/123	3.1	3.90
52	18-02-2004	14:26:02	46.63	6.91	10	3.5	3.3	4	65/143	3.0	4.98
53	18-02-2004	14:31:59	46.67	6.81	10	3.8	3.5	5	69/180	3.1	4.52
54	14-05-2004	00:30:35	45.03	7.48	10	4.0	3.6	19	66/174	3.4	2.89
55	12-06-2004	04:44:35	45.78	6.88	10	3.7	3.2	8	34/108	3.0	4.32
56	03-12-2004	22:28:59	44.34	7.35	5	3.1	3.1	5	81/155	2.8	6.48
57	25-03-2005	23:19:28	44.48	7.27	5	3.9	3.5	20	37/202	3.5	3.30
58	02-04-2005	04:33:52	44.75	6.76	5	3.5	3.1	17	18/150	3.2	3.83
59	10-04-2005	08:04:38	45.36	6.56	5	3.8	3.4	14	20/93	3.2	2.60
60	12-06-2005	21:16:15	45.11	7.35	5	3.3	3.1	9	54/173	3.0	4.30
61	08-09-2005	11:27:18	46.01	6.87	10	5.3	4.9	22	41/329	4.4	1.14
62	08-09-2005	11:53:11	46.02	6.88	5	3.5	3.2	5	40/88	2.7	7.55
63	08-09-2005	14:10:03	46.00	6.82	5	3.5	3.2	6	39/118	3.0	3.92
64	10-09-2005	13:25:29	44.60	6.87	5	3.6	3.2	9	38/168	3.3	2.43

Table 1. *(Continued)*

Number	Date	Hour	Latitude	Longitude	Depth (km)	M_{ldg}	M_{ren}	Number of records	Distance range (km)	M_w	f_c
65	04-10-2005	13:37:15	44.38	7.23	5	3.0	3.0	9	26/92	2.8	6.72
66	31-10-2005	03:39:58	45.68	6.40	5	4.1	3.6	17	31/243	3.2	2.88
67	20-12-2005	23:57:34	44.10	6.99	5	3.8	3.5	15	19/219	3.7	0.66
68	11-01-2006	10:32:08	45.92	5.41	5	4.1	3.7	7	19/280	3.5	1.43
69	02-09-2006	01:21:31	43.92	7.59	10	4.3	4.0	17	20/248	3.8	2.61
70	11-09-2006	15:04:11	44.70	7.80	5	3.7	3.3	11	71/187	3.2	5.70
71	24-10-2006	17:31:49	43.92	7.59	5	3.8	3.6	12	17/185	3.3	3.76
72	22-11-2006	15:54:32	45.83	6.68	6	3.3	3.0	10	26/97	2.7	6.51

Note: Date and localization are from the RéNaSS network. M_{ldg} and M_{ren} are local magnitudes from LDG and RéNaSS. The number and the distance range of recordings are also indicated, as well as the moment magnitudes and corner frequencies determined in this study.

Table 2. Same as Table 1 for the Rhine Graben.

Number	Date	Hour	Latitude	Longitude	Depth (km)	M_{ldg}	M_{ren}	Number of records	Distance range (km)	M_w	f_c
1	13-11-2000	16:30:40	47.21	7.58	11	3.8	3.6	4	42/117	3.2	5.25
2	22-02-2003	20:41:05	48.31	6.66	10	5.9	5.4	9	36/140	4.5	1.98
3	22-02-2003	20:54:25	48.32	6.68	10	3.7	3.4	3	38/87	3.1	6.46
4	23-02-2003	04:53:47	48.30	6.66	10	3.4	3.2	8	34/104	2.8	6.25
5	24-02-2003	00:35:41	48.30	6.65	10	3.3	3.1	5	34/89	2.7	7.11
6	04-03-2003	19:08:11	48.33	6.66	10	3.6	3.4	6	38/97	2.9	7.68
7	22-03-2003	13:36:17	48.19	8.91	5	4.8	4.5	5	122/171	3.9	2.69
8	24-03-2003	07:54:22	47.68	6.72	10	3.6	3.4	7	26/70	3.0	8.45
9	06-05-2003	21:59:46	46.97	8.81	5	4.2	3.8	7	127/200	3.4	3.71
10	24-08-2003	12:43:40	47.76	7.94	10	3.1	3.1	4	47/144	2.7	13.21
11	31-08-2003	05:38:57	47.56	7.88	10	3.3	3.1	5	27/105	2.9	11.15
12	16-02-2004	09:58:27	48.34	6.66	10	3.5	3.3	7	39/143	2.9	7.50
13	18-02-2004	14:26:02	46.63	6.91	10	3.5	3.3	3	126/178	3.0	6.83
14	18-02-2004	14:31:59	46.67	6.81	10	3.8	3.5	5	59/175	3.1	5.62
15	23-02-2004	17:31:21	47.30	6.28	10	5.5	5.1	9	26/181	4.2	3.37
16	13-03-2004	20:00:18	48.01	7.95	10	3.5	3.3	8	55/161	2.9	7.96
17	21-06-2004	23:10:02	47.50	7.67	21	-	3.8	8	25/115	3.4	5.41
18	28-06-2004	23:42:29	47.54	8.14	20	4.2	4.1	8	57/148	3.5	5.86
19	05-12-2004	01:52:39	48.11	8.00	10	5.2	4.9	8	55/171	4.1	3.40
20	12-05-2005	01:38:05	47.29	7.63	10	4.3	3.9	6	43/110	3.5	6.24
21	13-05-2005	19:44:07	48.07	8.02	10	3.5	3.2	7	61/169	2.9	8.73
22	03-11-2005	00:18:07	48.29	7.43	5	3.8	3.3	3	22/159	3.0	3.25
23	12-11-2005	19:31:16	47.52	8.14	10	4.3	3.8	3	106/147	3.3	7.72

with vertical incidence are shown in Fig. 2. We assume here that a v_{s30} of 2000 m s^{-1} is representative of hard rock sites for France.

In addition to eq. (5), a reference condition is also needed to remove the trade-off between seismic moments and site effects, which are the two constant parameters that control the amplitude of the spectrum (Andrews 1986; Field & Jacob 1995). As in Drouet *et al.* (2008a), we impose that the average of the logarithms of the site effects at each frequency over a number of stations is 0.

$$\sum_{j \text{ in list of reference stations}} s_{jk} = 0; \quad for\ all\ k. \tag{9}$$

The 'list of reference stations' has to be defined: the common practice is to use either all the stations, or a subset of stations located on rock. We choose the second option, beginning by identifying the rock stations. In a first inversion, we use all the stations within the reference list. From the obtained results, the stations showing the least amplification, and with a reasonably flat response, are identified as rock sites and kept in the final list of reference stations. The final inversion is then performed, using this additional information.

A system of equations must then be solved where the unknowns are the following: the m_{0_i} value (related to seismic moment) and the corner frequency f_{c_i} for each event i; the site term s_{jk} for each station j and each frequency k and the attenuation parameters Q_0, α and γ.

We use an iterative Gauss–Newton inversion scheme, based on the derivatives of y_{ijk} with respect to the parameters, to linearize the problem at each iteration and converge to the solution (Tarantola 2004; Drouet *et al.* 2008a).

4 RESULTS

4.1 Residuals

Fig. 3 shows the residuals (difference between the logarithms of observed and modelled amplitudes) for all the records and all the frequencies obtained after the inversion for the three regions (top of Fig. 3). The residuals from the three regions are combined in the bottom frames of Fig. 3. The amount of data is about the same for the Alps and the Pyrenees, whereas it is about three times smaller for the Rhine Graben. However, the distributions still have the same shape and also have similar standard deviations, that is, $\sigma = 0.26$,

Table 3. Same as Table 1 for the Pyrenees.

Number	Date	Hour	Latitude	Longitude	Depth (km)	M_{ldg}	M_{ren}	Number of records	Distance range (km)	M_w	f_c
1	04-06-2001	19:17:57	43.01	0.16	10	3.6	3.6	3	50/191	3.5	9.44
2	12-12-2001	12:10:52	43.12	−1.08	9	3.3	3.5	3	31/93	3.3	12.64
3	14-12-2001	18:28:54	42.87	−0.81	2	3.5	3.6	5	26/115	3.3	4.85
4	16-05-2002	14:56:33	42.94	−0.16	10	4.8	4.8	12	18/251	4.0	4.92
5	16-05-2002	15:14:44	42.82	−0.15	10	4.4	4.2	11	16/249	3.8	6.00
6	19-05-2002	04:44:13	42.99	0.15	10	3.8	3.8	10	22/198	3.4	7.23
7	11-06-2002	18:56:40	41.88	2.73	5	3.0	3.0	5	64/106	2.8	10.14
8	13-06-2002	10:42:32	41.86	2.78	5	3.2	3.4	6	68/130	3.0	11.01
9	21-06-2002	02:26:30	41.86	2.72	5	3.7	3.6	11	66/251	3.5	6.67
10	08-07-2002	09:46:48	42.99	−0.34	10	3.3	2.8	4	17/77	3.1	7.69
11	05-09-2002	20:42:15	43.05	−0.40	10	4.1	4.1	6	39/239	3.5	5.41
12	09-12-2002	13:44:54	43.02	0.19	5	3.7	3.3	5	21/191	3.2	7.14
13	11-12-2002	20:09:52	43.04	−0.33	5	4.3	4.4	5	24/153	3.8	4.99
14	12-12-2002	17:59:49	43.11	−0.28	10	4.9	4.6	9	15/263	4.0	4.87
15	13-12-2002	06:00:23	43.06	−0.28	5	3.3	2.9	4	20/150	2.9	10.95
16	16-12-2002	16:20:26	42.58	0.33	10	3.3	3.3	7	43/173	3.0	6.84
17	18-12-2002	17:58:08	43.00	0.21	10	3.2	2.4	5	25/109	2.9	8.15
18	21-01-2003	18:00:59	43.05	−0.36	10	4.6	4.4	11	28/277	3.8	5.16
19	26-02-2003	03:32:58	42.38	2.12	10	4.4	4.1	14	28/246	3.8	4.12
20	10-03-2003	00:54:38	42.39	2.14	10	3.1	3.0	6	27/101	2.8	6.91
21	03-10-2003	23:40:18	42.73	2.07	10	3.5	3.5	9	38/158	3.0	7.74
22	26-10-2003	08:28:32	41.88	2.76	5	3.0	3.3	3	65/89	2.9	10.03
23	03-02-2004	21:16:14	42.70	0.86	10	3.7	3.7	13	25/188	3.3	6.65
24	01-06-2004	16:50:19	42.39	2.17	5	4.4	4.1	6	33/109	3.5	4.24
25	04-06-2004	04:56:51	42.40	2.19	5	3.5	3.6	7	21/97	3.2	5.28
26	18-07-2004	02:16:02	42.92	1.04	10	3.8	3.7	12	15/178	3.5	5.55
27	22-07-2004	20:15:59	43.01	0.14	10	3.4	3.1	6	20/115	2.9	9.58
28	18-09-2004	12:52:15	42.78	−1.60	2	5.2	5.3	14	51/380	4.6	1.78
29	18-09-2004	19:58:29	42.94	−1.34	5	3.5	3.7	3	25/125	3.3	3.45
30	21-09-2004	15:48:05	42.34	2.02	5	5.1	4.8	14	45/239	4.2	2.94
31	21-09-2004	18:12:49	42.32	2.15	5	2.9	3.0	6	17/82	2.7	9.34
32	23-09-2004	09:50:18	42.31	2.13	10	3.5	3.5	7	20/108	3.2	5.05
33	23-09-2004	09:58:06	42.40	2.07	10	4.0	3.9	9	39/170	3.5	5.14
34	30-09-2004	13:09:05	42.77	−1.45	10	4.6	5.2	8	47/243	4.1	2.30
35	07-10-2004	06:16:29	42.83	−1.45	5	3.9	3.9	4	67/242	3.7	3.32
36	27-11-2004	22:22:02	43.04	−0.08	10	3.7	3.5	8	22/211	3.2	7.50
37	02-12-2004	18:11:18	41.61	2.45	5	3.3	3.5	5	99/152	3.2	5.91
38	15-01-2005	07:13:06	42.76	0.79	10	3.6	3.7	12	19/141	3.4	8.30
39	09-02-2005	15:20:45	42.01	2.58	10	3.5	3.7	6	66/124	3.2	6.78
40	15-02-2005	16:31:12	42.99	0.20	5	3.3	3.4	7	23/110	3.0	10.54
41	26-02-2005	20:36:49	42.62	0.83	5	3.7	3.7	17	27/189	3.4	6.70
42	15-06-2005	21:27:50	43.04	−0.67	5	3.5	3.5	8	21/258	3.3	8.22
43	17-06-2005	04:06:48	43.04	−0.21	5	3.3	3.0	5	15/144	2.9	10.10
44	16-07-2005	09:52:53	43.40	−0.63	5	3.5	3.4	3	34/59	3.4	2.03
45	05-11-2005	00:30:08	42.91	0.13	5	3.7	3.5	8	25/192	3.5	8.30
46	27-12-2005	21:33:22	42.36	1.43	5	3.8	3.8	10	47/140	3.4	3.90
47	07-02-2006	14:59:19	42.49	1.74	5	3.7	3.8	7	27/76	3.2	5.83
48	24-03-2006	07:19:20	42.80	2.55	5	3.1	3.3	5	23/60	2.9	7.08
49	29-03-2006	12:44:57	43.14	−0.63	5	3.3	3.3	4	18/60	3.2	6.64
50	04-05-2006	09:13:05	42.98	−0.70	5	3.3	3.3	4	26/73	3.3	5.71
51	04-05-2006	09:42:06	43.03	−0.70	5	3.4	3.6	5	24/73	3.4	6.70
52	08-05-2006	21:47:56	42.83	2.10	5	3.6	3.6	6	36/123	3.2	6.71
53	20-05-2006	05:36:06	43.00	0.00	5	3.7	3.5	7	16/161	3.2	6.75
54	02-06-2006	08:41:55	43.08	−0.28	5	3.5	3.2	4	19/39	3.0	7.73
55	25-07-2006	19:10:37	42.59	2.11	5	2.9	3.1	4	26/84	2.7	8.30
56	04-09-2006	05:44:22	42.45	1.65	5	3.0	3.0	3	39/58	2.9	7.08
57	24-10-2006	00:04:12	43.50	−0.62	5	3.6	3.2	6	29/65	3.4	3.41
58	04-11-2006	16:44:57	43.22	−0.31	6	3.8	3.8	5	17/42	3.4	6.30
59	14-11-2006	07:40:09	43.06	−0.65	11	3.2	3.0	5	21/67	3.0	6.11
60	17-11-2006	18:19:50	43.08	0.01	11	5.4	4.9	17	16/213	4.5	2.88
61	18-11-2006	20:34:19	42.98	0.01	6	3.6	3.1	8	15/125	3.2	6.10
62	18-11-2006	22:17:27	42.98	0.00	6	3.3	3.1	8	15/126	3.0	7.81

Table 3. *(Continued)*

Number	Date	Hour	Latitude	Longitude	Depth (km)	M_{ldg}	M_{ren}	Number of records	Distance range (km)	M_w	f_c
63	19-11-2006	13:16:12	43.00	0.00	6	3.5	3.2	8	15/126	3.2	7.00
64	20-11-2006	04:01:45	43.01	0.00	6	3.2	3.0	6	25/60	3.0	9.29
65	16-12-2006	08:17:01	42.99	−0.13	5	4.1	4.1	11	18/214	3.6	6.67
66	22-12-2006	12:14:58	43.46	−0.56	5	3.5	3.2	6	23/74	3.3	4.22

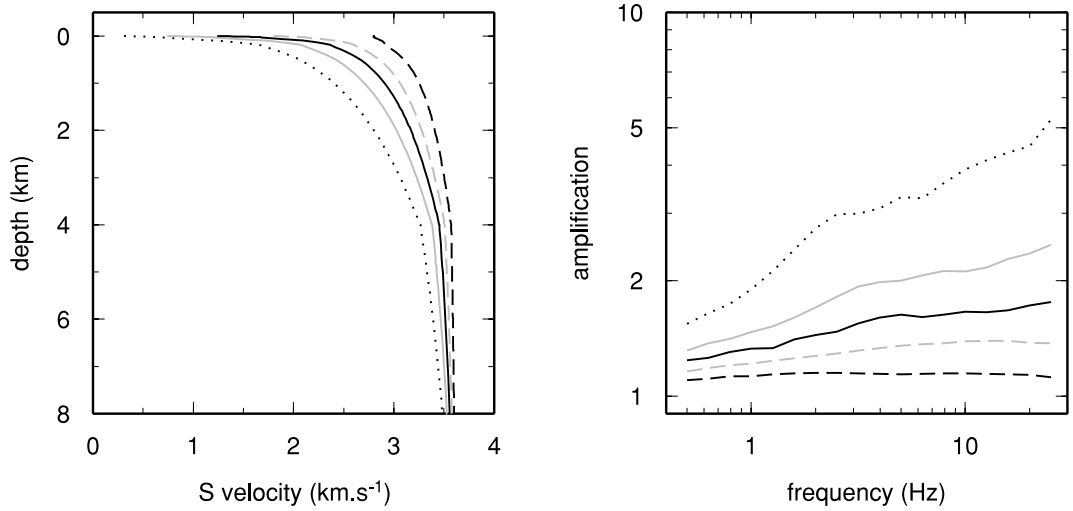

Figure 2. Left-hand side: generic rock velocity profiles (e.g. Boore & Joyner 1997; Cotton *et al.* 2006) with different v_{s30} values: 500 m s^{-1} (black dotted line), 1000 m s^{-1} (grey line), 1500 m s^{-1} (black line), 2000 m s^{-1} (grey dashed line) and 3000 m s^{-1} (black dashed line). Right-hand side: generic amplifications resulting from the profiles on the left for vertically incident *SH* waves, using a Haskell–Thomson procedure.

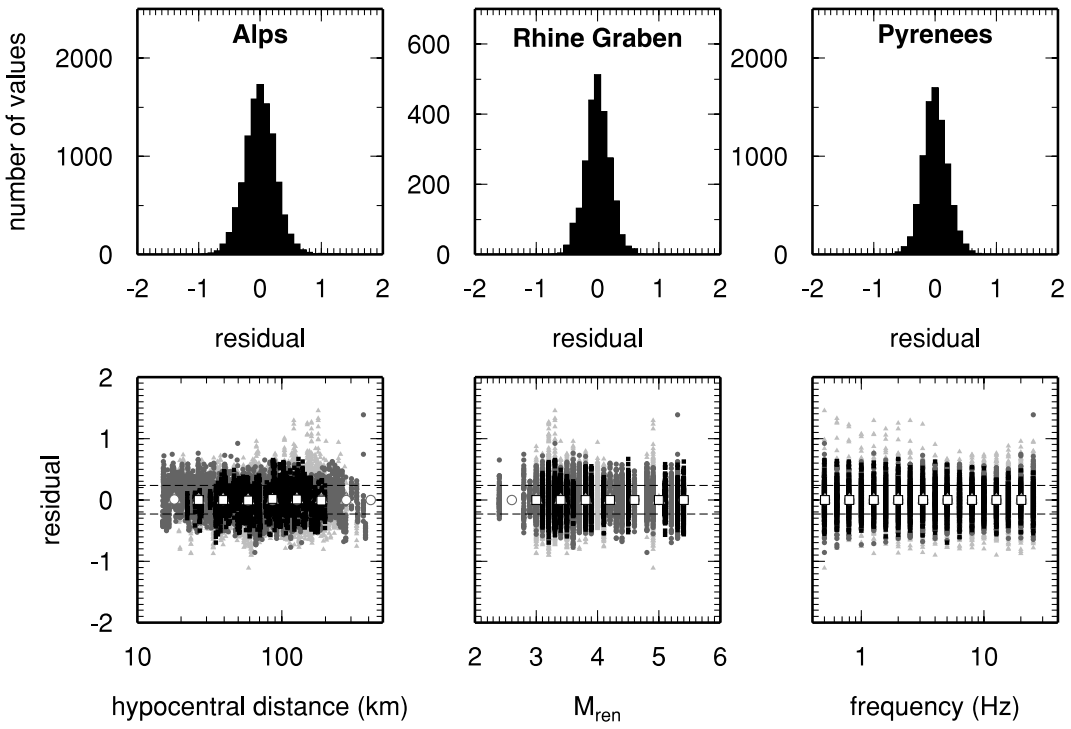

Figure 3. Top panels: distributions of residuals for each region after the inversion. Bottom panels: plots of the residuals (Alps: light grey triangles, Rhine Graben: black squares and Pyrenees: grey circles) as a function of distance (left-hand panel), local magnitude (middle panel) and frequency (right-hand panel). Dashed lines show the one standard deviation of the whole residuals distribution. Large white filled symbols are average residuals over a number of distances, magnitude and frequency bins.

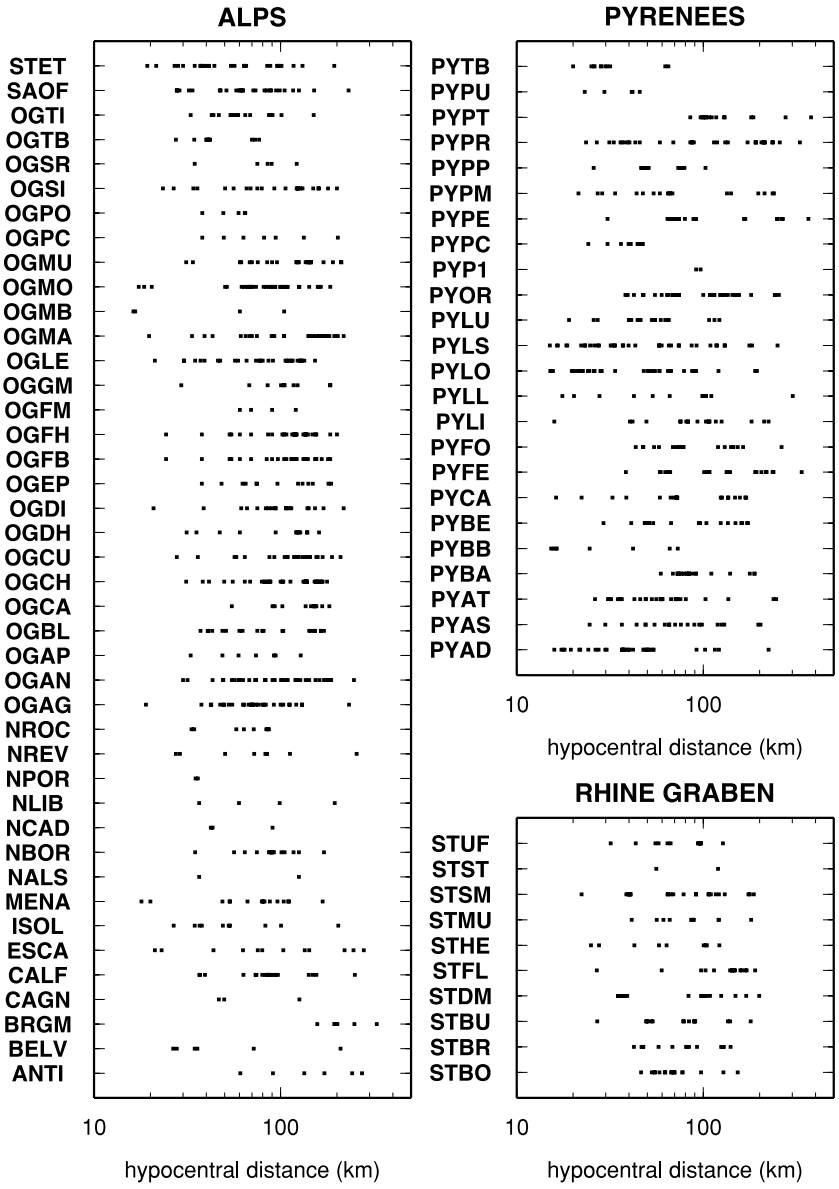

Figure 4. Hypocentral distance distribution at the stations in each region.

0.20 and 0.20, for the Alps, the Pyrenees and the Rhine Graben, respectively.

At the bottom of Fig. 3 the residuals are plotted as function of the distance, the magnitude and the frequency for the three data sets. The standard deviation computed for the three data sets simultaneously is $\sigma = 0.23$. Fig. 4 shows that the distance distribution is fairly homogeneous at each station for the three regions. Figs 3 and 4 show that there is no obvious trend for the residuals with either distance, magnitude or frequency, indicating that no bias is included during the inversion process.

4.2 Regional attenuations

The results for the three attenuation parameters γ, Q_0 and α are given in Table 4 for the three regions. The standard deviations are relatively small, except for Q_0 and α in the Rhine Graben where the limited number of recordings lead to higher uncertainty in the attenuation parameters.

Table 4. Inverted attenuation parameters.

Region	γ	Q_0	α
Alps	1.06 ± 0.01	336 ± 15	0.32 ± 0.02
Rhine Graben	1.06 ± 0.01	1163 ± 247	0.19 ± 0.07
Pyrenees	1.19 ± 0.01	790 ± 31	0.15 ± 0.01

Those attenuation parameters, especially the Q values, are the most difficult parameters to invert because small variations of Q_0 and α lead to almost unchanged amplitudes, mainly at low frequency and short distance. The main attenuation models valid for the investigated regions that were found in the literature are: Thouvenot (1983) ($Q_0 = 436$, $\alpha = 0.25$) and Drouet *et al.* (2008a) ($Q_0 = 322$, $\alpha = 0.2$) for the Alps; Modiano & Hatzfeld (1982) ($Q_0 = 250$, $\alpha = 0.0$), Gagnepain-Beyneix (1987)1 ($Q_0 = 30$, $\alpha = 1.1$), Gagnepain-Beyneix (1987)2 ($Q_0 = 142$, $\alpha = 0.7$) and Drouet *et al.* (2008a) ($Q_0 = 376$, $\alpha = 0.5$) for the Pyrenees. Two other models exist for the whole of France: Nicolas *et al.* (1982) ($Q_0 = 100$,

$\alpha = 0.8$) and Campillo & Plantet (1991) ($Q_0 = 320, \alpha = 0.5$). Note that the original model of Thouvenot (1983) is valid for P waves ($Q = 756 \times f^{0.25}$), and it was converted assuming $Q_S = Q_P/\sqrt{3}$ and $\alpha_S = \alpha_P$.

To test the adequacy of the attenuation models, we filtered the times-series for each earthquake in each region around four central frequencies: 1, 5, 10 and 25 Hz. The peak ground acceleration (PGA) values for the east–west and north–south components, corrected for the Brune's source model using the inverted seismic moments and corner frequencies, and scaled to have amplitude 1 at 40 km, are plotted against distance in Fig. 5. The attenuation models: $\exp[-\pi f R_{ij}/(Q_0 f^{\alpha} v_S)]/R_{ij}^{\gamma}$ using γ-values from Table 4 together

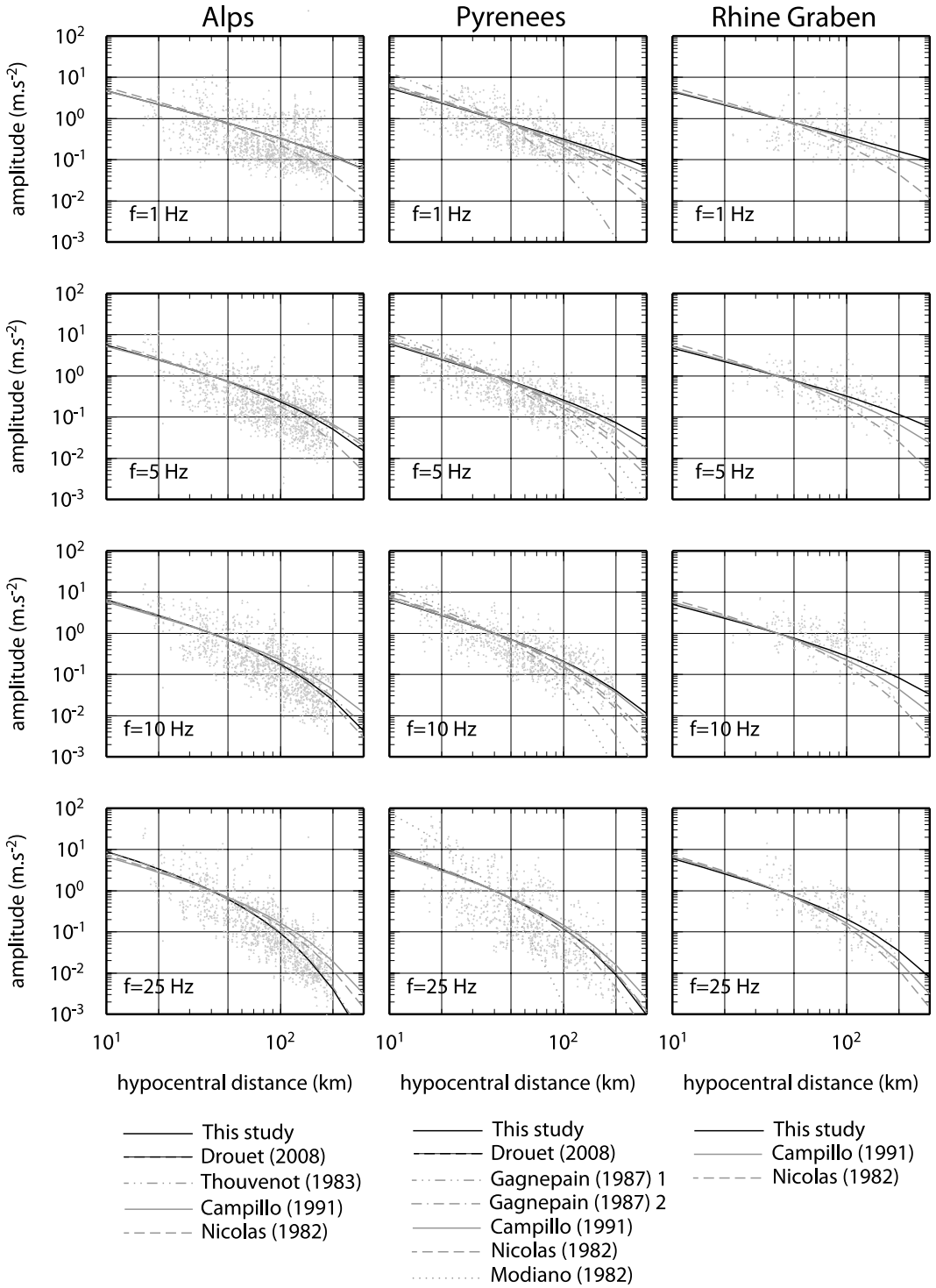

Figure 5. Peak-ground acceleration of the filtered time-series (east–west: triangles; north–south: circles) for four different frequencies in each region. The attenuation models are the Q-models described in the text, associated with the γ-values of Table 4. Note that the amplitudes are scaled to get an amplitude equal to 1 at 40 km.

with Q_0- and α-values from Table 4 or from the literature are also plotted in Fig. 5. These results show that most of the models fit equally well the data.

Looking at Fig. 5, we can however draw some conclusions concerning the different models. Models with a low Q_0 (below 300) and no frequency dependence lead to an overestimation of attenuation for the high frequencies at long distance, for example, Modiano & Hatzfeld (1982) for the Pyrenees at 25 Hz. The same conclusion would be observed for the Alps and the Rhine Graben, should such models exist, suggesting that Q is frequency dependent. One can also reject models with a frequency dependence greater than 1, for example, the first model by Gagnepain-Beyneix (1987) leads to lower attenuation at high frequency than at low frequency, which is opposite to the usual observations in this frequency band (0.5–30 Hz). The Nicolas *et al.* (1982) model gives a slight overestimation of attenuation at low frequencies but gives an overall reasonable fit. Consequently, we suggest an upper bound of 0.8 for the frequency dependence in the three regions if it is associated with a low Q_0. Our analysis also supports the idea that the frequency dependence is higher in the Alps than in the other two regions, as shown by the data in Fig. 5.

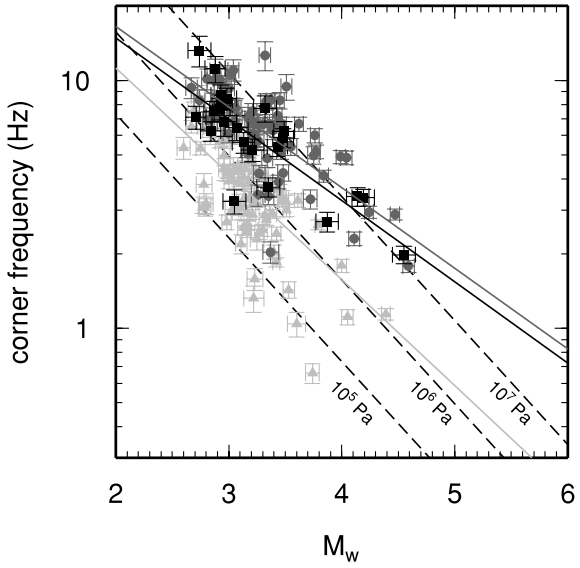

Figure 7. Corner frequencies as a function of moment magnitudes. Solid lines show the regressions determined in this study for the Alps (light grey), the Rhine Graben (black) and the Pyrenees (dark grey). Dashed lines show constant stress drops of 0.1, 1 and 10 MPa (1, 10 and 100 bars).

4.3 Source parameters

Moment magnitudes are determined from the seismic moments using the Hanks & Kanamori (1979) relationship

$$M_w = \frac{\log_{10}(M_0) - 9.1}{1.5}. \quad (10)$$

Fig. 6 shows a comparison of the moment magnitude scale determined in this study and two local magnitude scales used in France (M_{ldg} and M_{ren}). The solid black lines show the regressions obtained in this study

$$M_w = 0.42(\pm 0.10) + 0.77(\pm 0.03) \times M_{ldg} \quad (11)$$

$$M_w = 0.43(\pm 0.10) + 0.80(\pm 0.03) \times M_{ren}. \quad (12)$$

Those relations are close to that obtained by Drouet *et al.* (2008a), which are also shown in Fig. 6.

To test our moment magnitude scale, we search through the catalogue of the Swiss Seismological Service (http://www.seismo.ethz.ch/) for the events where a moment magnitude has been computed using the waveform inversion technique of surface waves. Fig. 6 displays the comparison for the 29 earthquakes for which the information was available. It shows that from magnitude 3 to 5, the two independent methods give equivalent values. The regression between the two magnitude scales gives

$$M_w = 0.24(\pm 0.16) + 0.90(\pm 0.05) \times M_{w\text{-ETH}}. \quad (13)$$

Fig. 7 shows the corner frequencies as a function of the moment magnitudes. Lines of constant stress drop of 0.1, 1 and 10 MPa (1, 10 and 100 bars) are indicated. In this case, a regional dependence of the relationship between corner frequency and moment magnitude is apparent. The regression give the following relationships for the three different regions:

$$Alps : \log_{10}(f_c) = 1.91(\pm 0.08) - 0.43(\pm 0.03) \times M_w, \quad (14)$$

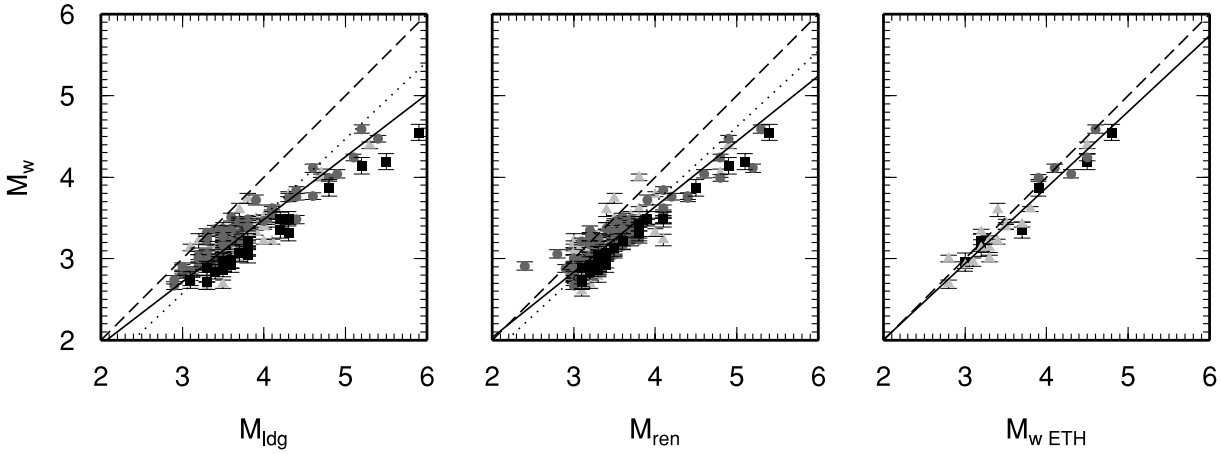

Figure 6. Inverted moment magnitudes as a function of LDG local magnitudes (left-hand panel), ReNaSS local magnitudes (middle panel) and ETH moment magnitudes (right-hand panel), for the Alps (light grey triangles), the Rhine Graben (black squares) and the Pyrenees (grey circles). Solid lines show the regressions determined in this study, dotted lines show the regressions from Drouet *et al*. (2008a) and dashed lines correspond the one-to-one relationship.

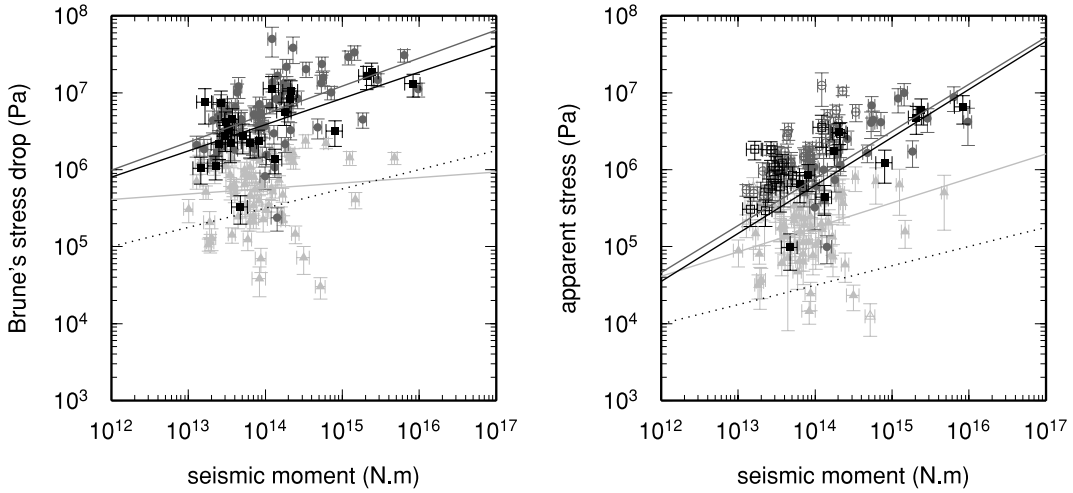

Figure 8. Brune's stress drops as a function of seismic moments (left-hand panel), and apparent stresses as a function of seismic moments (right-hand panel). Solid lines show the regressions determined in this study for the Alps (light grey), the Rhine Graben (black) and the Pyrenees (dark grey). Dotted lines show the dependency of $\Delta\sigma$ and σ_a on seismic moment [originally developed for σ_a: $\sigma_a \propto M_0^{0.25}$ Mayeda & Walter (1996) and extrapolated to $\Delta\sigma$ assuming proportionality between $\Delta\sigma$ and σ_a Bay *et al.* (2005)]. Open symbols in the right-hand frame do not fulfill the conditions $\frac{f_c}{2} \geq f_{\min}$ or $5 \times f_c \leq f_{\max}$ (see text).

$$RhineGraben : \log_{10}(f_c) = 1.83(\pm 0.14) - 0.33(\pm 0.04) \times M_{\rm w}, \quad (15)$$

$$Pyrenees : \log_{10}(f_c) = 1.87(\pm 0.08) - 0.33(\pm 0.02) \times M_{\rm w}. \quad (16)$$

The inverted moment magnitudes and corner frequencies for each earthquake are reported in Tables 1–3.

From the inverted seismic moments and corner frequencies, Brune's stress drops are computed using the Brune (1970) relationship.

$$\Delta\sigma = \frac{7}{16} M_0 \left(\frac{f_c}{0.37 v_S} \right)^3. \quad (17)$$

As a consequence of the regional dependence of the corner frequency–moment magnitude relationship, the mean stress drop values are also regionally dependent. The mean stress drop for the three data sets equals to 4.9 MPa (49 bars) whereas values of 0.9, 5.7 and 8.9 MPa (9, 57 and 89 bars) are found for the Alps, Rhine Graben and Pyrenees individually. The computed Brune's stress drops are shown in Fig. 8.

We also computed apparent stress, defined as

$$\sigma_a = \frac{2\mu E}{M_0}, \quad (18)$$

where E is the radiated seismic energy assumed to be equal the to S-wave radiated energy. In reality P waves also carry some radiated energy however this energy is estimated to be less than 10 per cent of the total energy (Abercrombie 1995; Mayeda & Walter 1996). Here, E will denote the S-wave energy. μ, the shear modulus, is taken as 3.4×10^{10} Pa.

E is estimated from the integration of the squared velocity source spectra (obtained by integration of the acceleration source spectra) in the frequency domain (Mayeda & Walter 1996)

$$E = \frac{R_{\theta\phi}}{4\pi\rho v_S^5} \times \int_{f_1}^{f_2} V(f)^2 {\rm d}f. \quad (19)$$

Here $V(f)$ is computed from the original data, corrected for site and propagation effects, and averaged for each earthquake over all the stations. As most of the energy is radiated at around the corner frequency, Abercrombie (1995) suggests that f_1 should be less than half the corner frequency and that f_2 should be greater than five times the corner frequency. Another study (Ide & Beroza 2001) computed a correction function to account for missing high frequencies in the integration which arises from recording limitations. The apparent stresses shown in Fig. 8 are all adjusted using the Ide & Beroza (2001) method; earthquakes which do not fulfill the condition proposed by Abercrombie (1995) are indicated as open symbols.

Standard deviations on Brune's stress drop are estimated from the corner frequency and seismic moment standard deviations. Similarly, standard deviations on apparent stress are estimated from the energy and seismic moment standard deviations. Note that the standard deviations of energy are relatively high. This is because they combine the uncertainty linked to source spectra retrieval (via path and site effects corrections) with the uncertainty from averaging the source spectra over all the stations.

Both Brune's stress drop and the apparent stress show an increase with increasing seismic moment (Fig. 8). The increase is almost linear in a log–log space and flattens towards higher values of seismic moment. If one extrapolates the results to high magnitudes, then unrealistically high stress drops would be obtained. Thus this flattening of the curves is expected. Mayeda & Walter (1996) have already observed a scaling of apparent stress with seismic moment: $\sigma_a \propto M_0^{0.25}$, which can be extrapolated to Brune's stress drop assuming proportionality between apparent stress and Brune's stress drop. The scalings observed here are of the same order of magnitude. One other interesting result is the regional dependence of the stress drop, which is lower in the Alps than in the other two regions. One possible explanation is the pre-dominant extensional regime in the Alps. This will be discussed later.

4.4 Site effects

4.4.1 Site transfer functions

As shown by previous studies, the site amplifications are the most stable parameters coming out of an inversion such as the one

presented in this paper, because they are less sensitive to the trade-off between parameters (Field & Jacob 1995; Drouet *et al.* 2008a). In addition, several studies (Field & Jacob 1995; Bonilla *et al.* 1997; Drouet *et al.* 2008a; Bindi *et al.* 2009) have shown similarities between the calculated site effects from an inversion method, and those computed using other common methods (such as the spectral ratios with reference station or the horizontal-to-vertical spectral ratios). More specifically, Drouet *et al.* (2008a) have shown a semblance of the site effects estimated from these different methods at stations PYLO and OGDH. The inversion results are also similar to the theoretical amplifications computed from a layered soil model in Drouet *et al.* (2008b).

The main difficulty is in defining the reference used. In this study, all the spectra have been corrected for crustal amplification using a generic rock site with a $v_{s30} = 2000\,\mathrm{m\,s^{-1}}$ as the reference. This methodology allows us to compare the site effects obtained from independent inversions (i.e. for the three regions). After a first trial inversion, the stations that are kept in the list of reference stations (as explained in section 3) are: CALF, ISOL, NBOR, OGAN, OGCH, OGFB, OGGM, OGLE, OGMU, SAOF and STET for the Alps; STSM for the Rhine Graben; PYAS, PYLI, PYLL and PYLO for the Pyrenees. Fig. 9 shows that no systematic bias with distance or magnitude affect the residuals obtained at the reference stations for two selected frequencies (1 and 10 Hz). Such bias would be observed

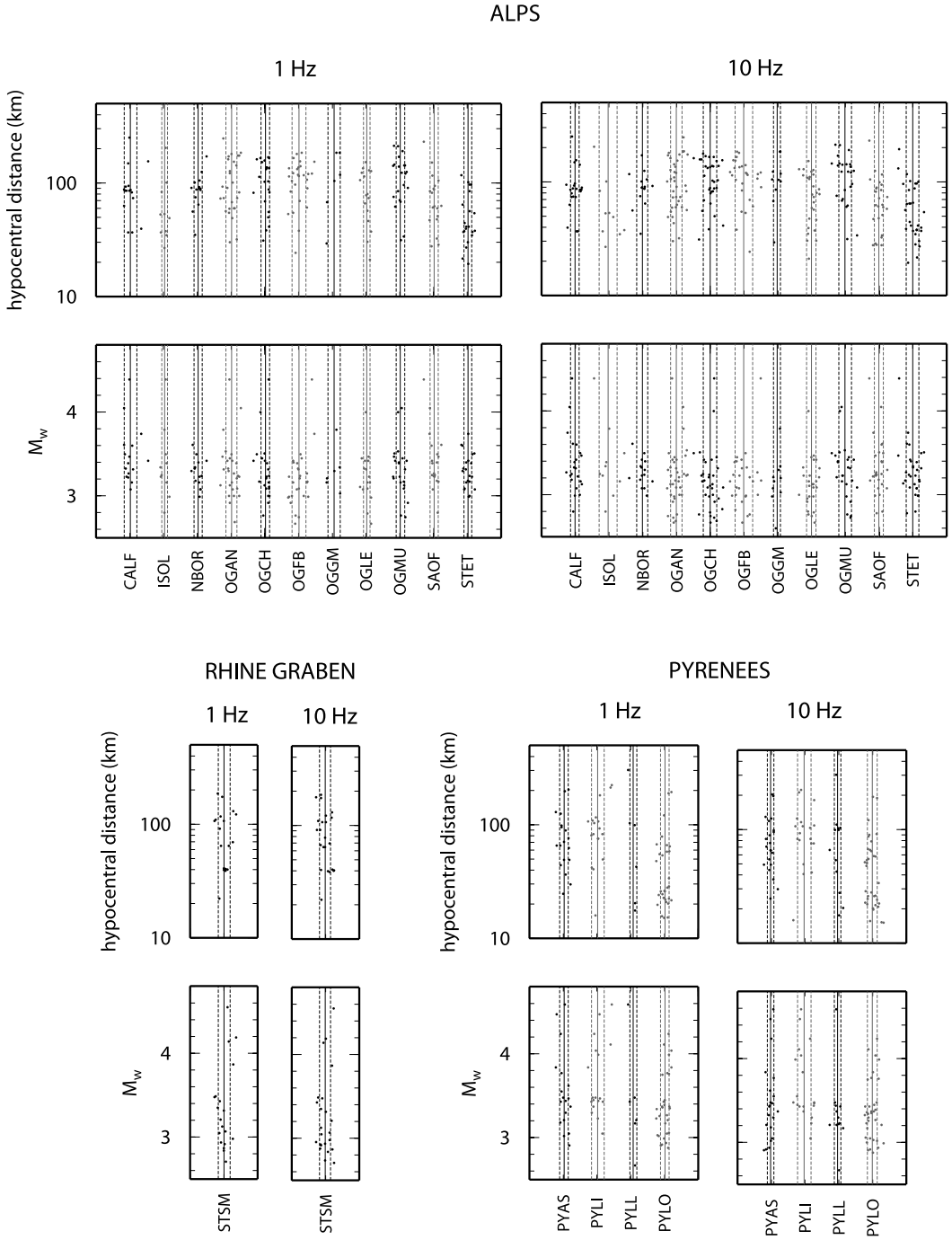

Figure 9. Distribution of the residuals versus hypocentral distance and magnitude for two frequencies: 1 and 10 Hz, for the reference stations in each region.

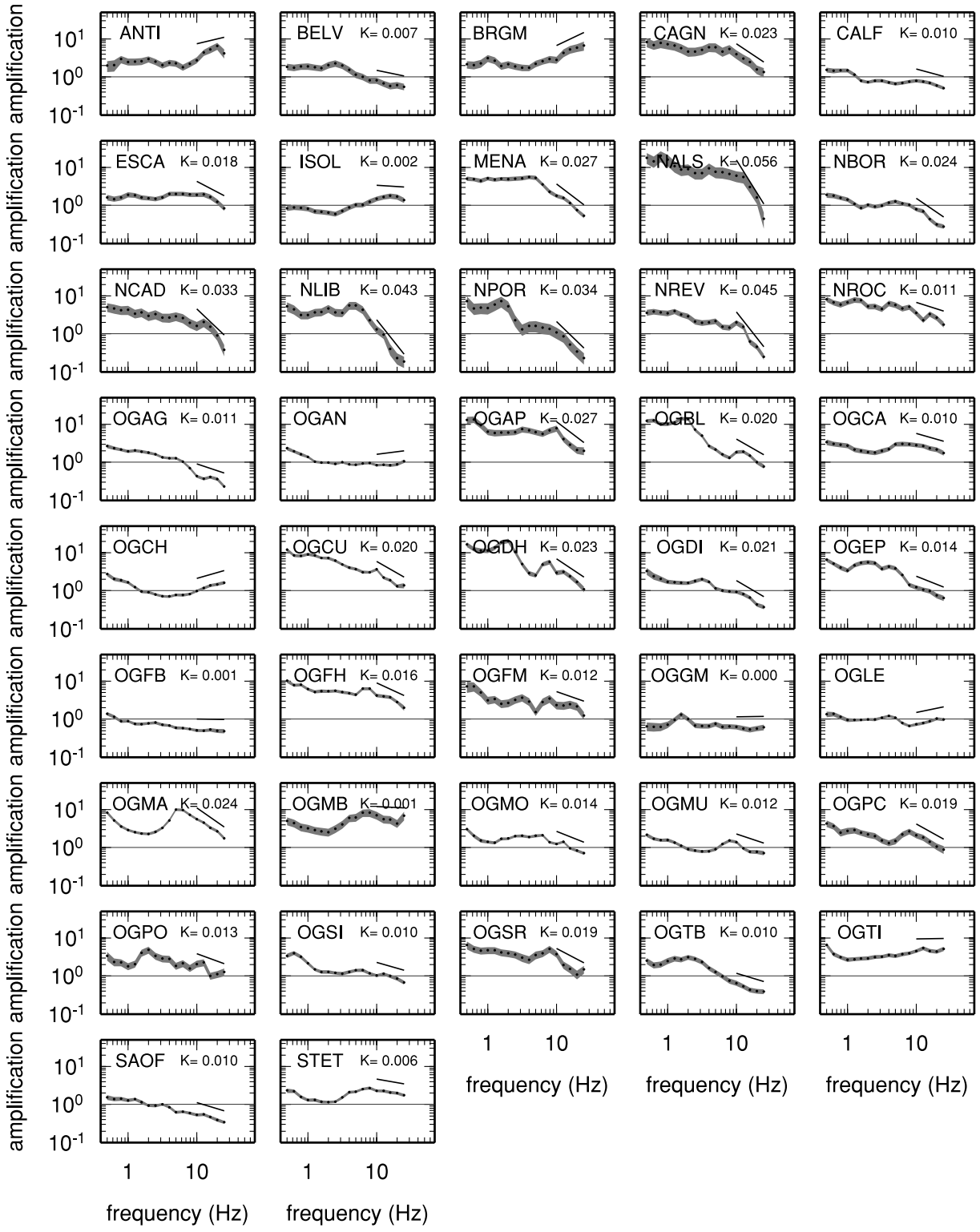

Figure 10. Site transfer functions ± one standard deviation for the horizontal component (black line and dark grey shaded area) for the stations in the Alps. Solid lines indicate the regression of the high frequency part of the transfer functions, which leads to the κ-values indicated on top of each frame.

if all the reference stations were affected by strong fall-offs at high frequencies.

Figs 10–12 show, for each region, the site transfer functions for the different stations. The largest amplifications in the frequency range 1–5 Hz are obtained for stations in the Alpine Valleys (e.g. NALS, NPOR, OGAP, OGBL, OGDH among others), reaching amplifications greater than 10. The stations in the Rhine Graben area present lower amplifications above 1 Hz, however Fig. 11 suggests that high amplification occurs at low frequency (below 1 Hz). This could be linked to a large-scale structure like the Rhine Graben. Some of the Pyrenean stations are also characterized by large amplifications below 10 Hz, however the most striking feature

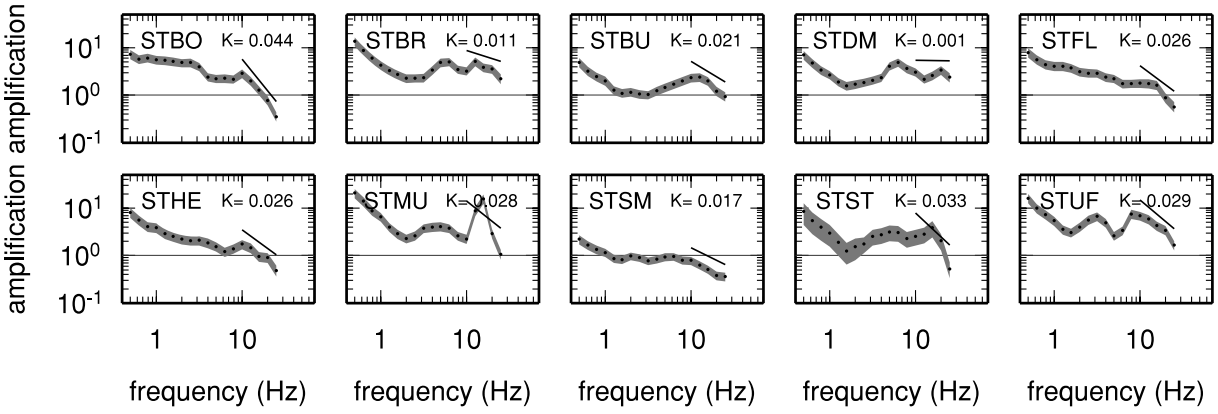

Figure 11. Same as Fig. 10 for the stations in the Rhine Graben.

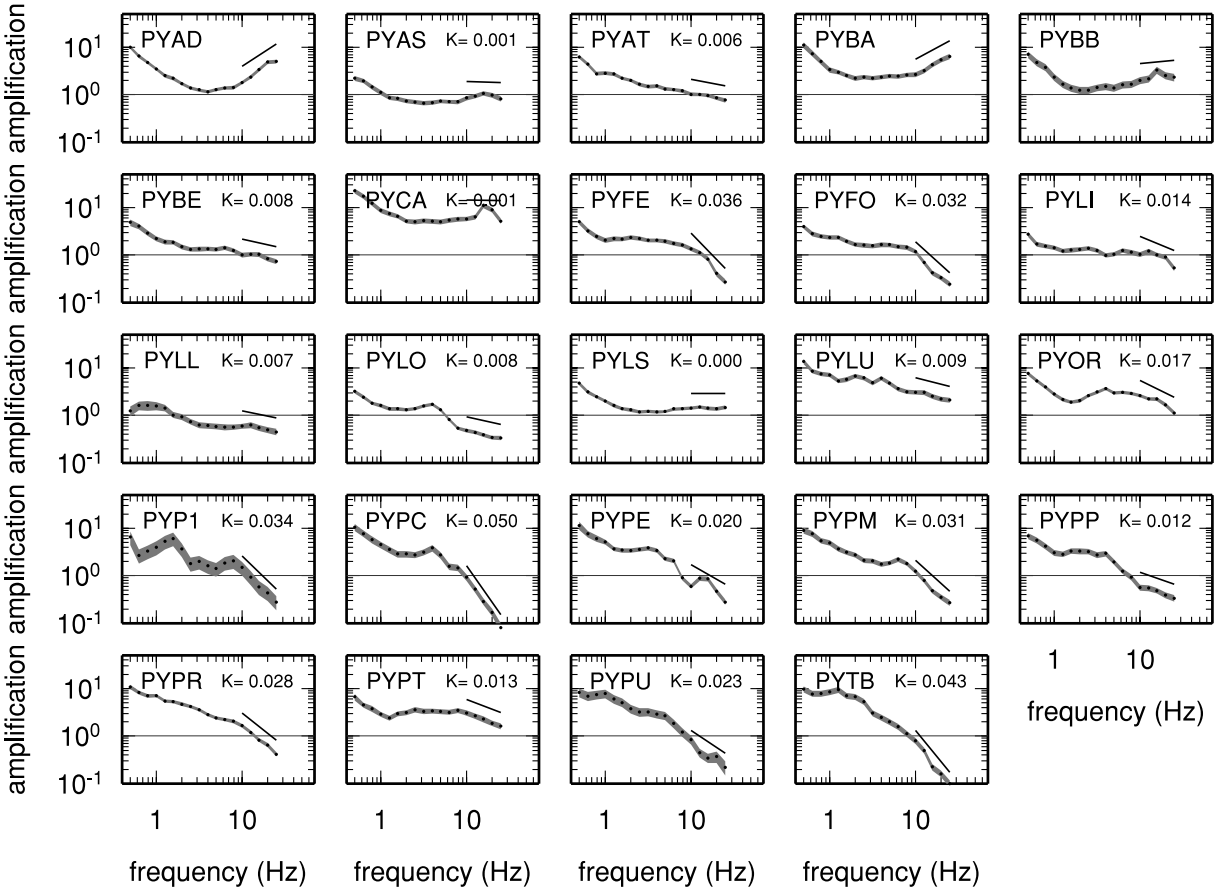

Figure 12. Same as Fig. 10 for the stations in the Pyrenees.

is the high attenuation observed at high frequencies (above 10 Hz) at most of the stations. Some studies have shown that scattering is very strong in this region (Gagnepain-Beyneix 1987) which could explain the observed rapid high-frequency decay.

4.4.2 Kappa (κ)

From these curves, we also compute the κ values by regression of the high-frequency part of the transfer functions ($f \geq 10$ Hz). Similar to Anderson & Hough (1984), we model the high-frequency attenuation through $\exp(-\pi \kappa f)$, however in our case the κ values are independent of distance since the inversion procedure has already accounted for this. The computed values of κ are indicated in Figs 10–12 next to the station name. For some of the stations, we see that the peaks in the transfer function are probably leading to a biased κ (e.g. NCAD, STST or PYPE). This effect has already been analysed theoretically by Parolai & Bindi (2004). For a few stations, the procedure also gave positive slopes, in which case no κ is computed because it would have been a negative value. However, for most of the stations, a good fit is obtained and the κ-values range between 0 and 0.05, which is the usual range of variation for κ.

The Anderson & Hough (1984) method has recently been applied to the French data by Douglas *et al.* (2010) and the results are summarized in Table 5. Although there is a clear correlation between the κ-values from both methods, ours are pre-dominantly lower,

Table 5. κ-values from Douglas *et al.* (2010) (from their constrained weighted regression, i.e. after correction for regional attenuation) compared to κ-values from this study.

Station	κ Douglas *et al.* (2010)	κ This study
OGMO	0.035	0.014
OGMU	0.027	0.012
OGSI	0.023	0.010
PYAT	0.016	0.006
PYFE	0.030	0.036
PYLO	0.021	0.008
PYLS	0.008	0.000
PYOR	0.015	0.017
PYPR	0.025	0.028

except for stations PYFE, PYOR and PYPR. The difference may be the result of data processing and attenuation correction. In our case, we first separate source, path and site effects using data for all the stations in the 0.5–30 Hz frequency band. Then in a second step, we estimate κ by regression of the high-frequency part ($\geq$10 Hz) of the site transfer functions. Douglas *et al.* (2010) used a higher frequency band from 2–12 to 20–50 Hz depending on the quality of the data to determine a κ_r which depends on distance, because it includes the effect of attenuation. They made attenuation correction at a regional scale using the slope of the κ_r distance curves, before the final κ-value for each station is computed. Consequently, the attenuation correction term is estimated using only high-frequency data in Douglas *et al.* (2010). Our results are also likely to be less affected by source effects, because again the inversion process deconvolves all the terms.

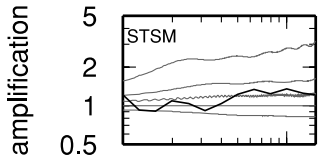

Figure 14. Same as Fig. 13 for the stations in the Rhine Graben.

4.4.3 v_{s30}

We develop a new method to infer some information about the mean shear wave velocity over the uppermost 30 m (v_{s30}). We have computed the ratios between the generic rock site amplifications for different v_{s30}-values (shown in Fig. 2) with respect to the generic rock site amplifications for $v_{s30} = 2000\ \mathrm{m\,s^{-1}}$. We then compare these ratios with the inverted site transfer functions (which are also relative to the generic rock site amplifications for $v_{s30} = 2000\ \mathrm{m\,s^{-1}}$), corrected for the κ effect. This comparison is shown for the rock stations in Figs 13–15. Then we assign to each rock station in France the v_{s30}-value that minimizes the misfit between the site transfer function and the generic amplification curves (see Table 6). A quality criteria, estimated visually, is also given in Table 6 which describes the level of confidence we give to the estimated v_{s30}-values ('+++' for a good fit, '++' for an intermediate fit and '+' for a poor fit).

Our results show that stations identified as rock stations from superficial geological investigations can be split in three categories depending on the v_{s30}-value: (1) soft rock: v_{s30} from 500 to 1000 $\mathrm{m\,s^{-1}}$; (2) intermediate rock: v_{s30} from 1000 to 2000 $\mathrm{m\,s^{-1}}$ and (3) hard rock: v_{s30} above 2000 $\mathrm{m\,s^{-1}}$. From Table 6 it is clear that stations located on alluvial deposits (BELV), or moraines (PYFO) are included in the soft-rock category. PYLO is an outlier located on Moraines but with a relatively high v_{s30}(1500 $\mathrm{m\,s^{-1}}$). This

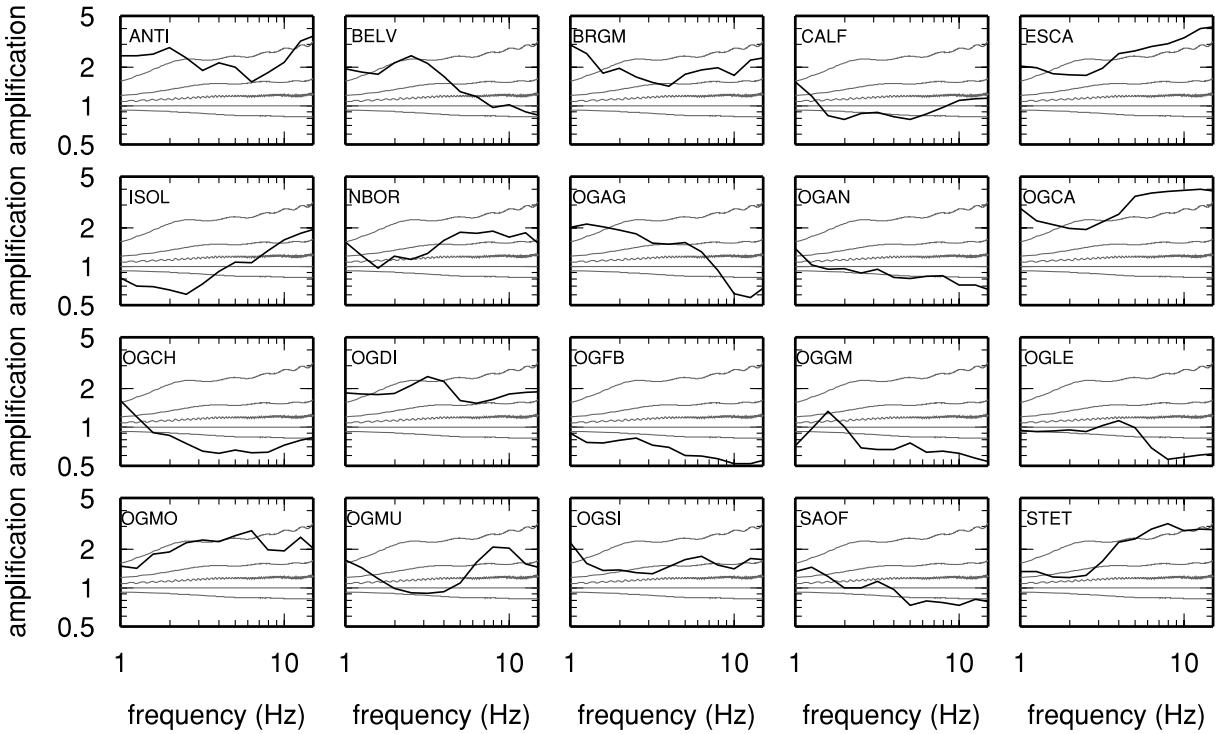

Figure 13. Site transfer functions for the rock stations in the Alps after correction of κ (black lines) compared with the ratios between generic amplifications for $v_{s30} = 500$, 1000, 1500, 2000 and 3000 $\mathrm{m\,s^{-1}}$ with respect to generic amplification for $v_{s30} = 2000\ \mathrm{m\,s^{-1}}$ (grey lines).

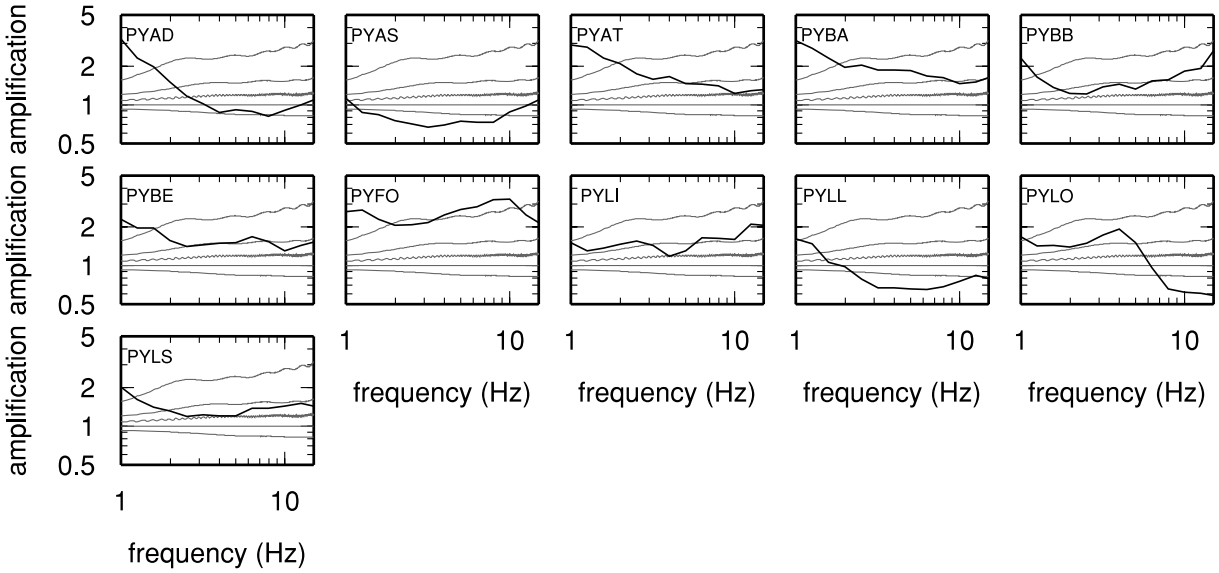

Figure 15. Same as Fig. 13 for the stations in the Pyrenees.

Table 6. v_{s30}-values determined from Figs 13 to 15.

Station	v_{s30} (m s^{-1})	Quality	Geology
Alps			
ANTI	500	++	Dolomites (Upper and Middle Jurassic)
BELV	1000	+	Alluvium (undetermined age)
BRGM	500	++	Limestone
CALF	2000	++	Limestone (Callovian)
ESCA	500	+++	Limestone (Senonian)
ISOL	2000	+	Metamorphic crystalline massifs
NBOR	1000	++	Limestone (Portlandian)
OGAG	1500	+	Limestone (Dogger)
OGAN	3000	+++	Limestone (Barremian, Aptian)
OGCA	500	+++	Limestone (Valanginian)
OGCH	3000	++	Limestone (Tithonian)
OGDI	500	++	Limestone (Hettangian, Sinemurian, Pliensbachian)
OGFB	3000	+++	
OGGM	3000	++	Limestone (Pliensbachian, Toarcian)
OGLE	3000	++	Metamorphic crystalline massifs
OGMO	500	+++	Gypseous formation (Triassic)
OGMU	1000	+	Limestone (Oxfordian, Kimmeridgian)
OGSI	1000	+++	Limestone (Barremian, Aptian)
SAOF	3000	++	Sandstone (Mesozoic)
STET	500	++	Rock fragments above metamorphic crystalline massifs
Rhine Graben			
STSM	1500	++	
Pyrenees			
PYAD	1500	+	Limestone (Aptian)
PYAS	3000	+++	Gneiss
PYAT	1000	++	Marlstone (Albian)
PYBA	500	++	Limestone
PYBB	1000	++	Flysh (Albian, Cemonian)
PYBE	1000	++	Marlstone (Albian)
PYFO	500	+++	Moraines (Würm)
PYLI	1000	+++	Limestone (Aptian)
PYLL	3000	++	Gneiss (Precambrian)
PYLO	1500	+	Moraines (Würm)
PYLS	1000	++	Calcareous schistose formation (Carboniferous)

station is located on a slope of a hill and topographic site effects have been observed (strong deamplification above 5 Hz, Dubos 2003). The stations located on metamorphic crystalline massifs (OGLE, ISOL) or on gneiss (PYAS, PYLL) are in the hard-rock category. One interesting station is STET, located on rock fragments above metamorphic crystalline massifs. As Fig. 13 shows, this station exhibits high amplification above 2–3 Hz, whereas the part of the curve below 2–3 Hz suggests a high v_{s30}. Finally, for the stations

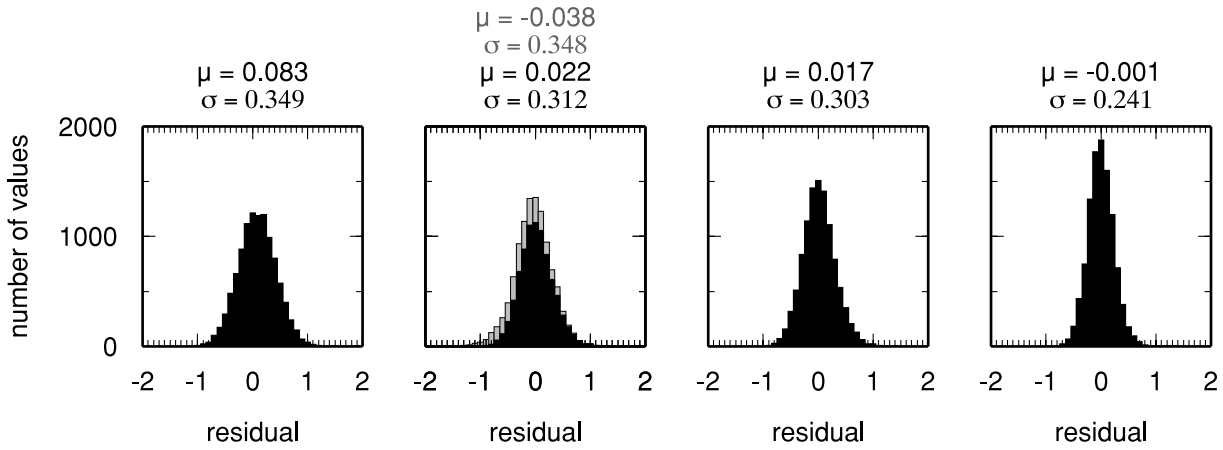

Figure 16. Distributions of residuals for the rock stations tabulated in Table 6, computed without site correction (first frame), using a site correction based on v_{s30} (second frame), using a site correction based on v_{s30} and κ (third frame) and with a site correction based on the inverted site amplification curves (fourth frame). On top of each frame, the median and standard deviation of the corresponding normal distribution are shown. The grey distribution in the second frame corresponds to all the frequencies while the black distribution results from frequencies lower than 10 Hz.

located on limestone, which appear in each of the rock categories, there is a large variability of the response.

To check the reliability of the v_{s30} estimates, we tried to quantify the reduction of the residuals linked with the use of these estimates as a proxy for site effects. We computed modelled spectra using the inverted seismic moments, corner frequencies and propagation parameters. Site effects were handled in four ways: no correction; correction using generic amplification curves based on the computed v_{s30} for each station; correction using generic amplification curves based on the computed v_{s30} for each station plus correction of κ and correction using the inverted site specific amplification curves. Fig. 16 shows the four distributions of residuals corresponding to these four cases. One can see the reduction in standard deviation at each step, from 0.35 without site correction to 0.24 with site specific site corrections. From Fig. 16 one can also see that the correction based on v_{s30} only improves the residuals below 10 Hz (median closer to zero and lower standard deviation), while the combined correction of v_{s30} and κ results in a global improvement for all the frequencies.

Finally, we compare the κ–v_{s30} couples we computed for the rock stations in France with the results obtained in California by Silva *et al.* (1998) (Fig. 17). The uncertainties linked with the estimation of both κ and v_{s30} are very high as shown by the error bars in Fig. 17. Looking at these results one cannot draw a clear conclusion about the correlation between kappa-values and v_{s30}. A recent paper by Campbell (2009) shows that the kappa-values are strongly dependent on the sediment thickness for soft sites. κ may thus also depend on deep structures at rock sites, which could explain the low level of correlation with v_{s30}, a value that describes superficial properties of the soil.

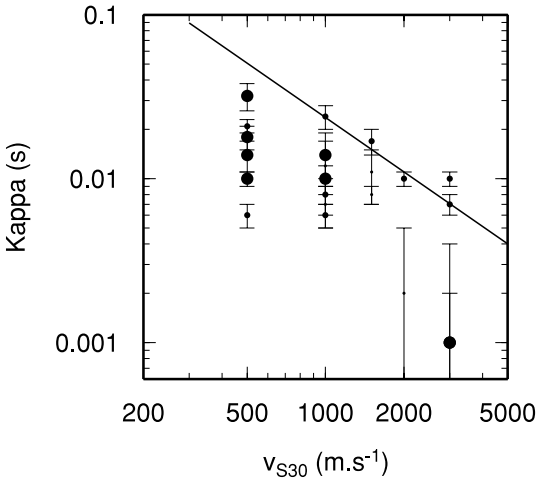

Figure 17. Plot of the v_{s30} versus the κ-values (circles) compared with the relationship derived by Silva *et al.* (1998). The size of the symbol refers to the quality of the v_{s30} as given in Table 6.

5 DISCUSSION AND CONCLUSION

We modified the method proposed by Drouet *et al.* (2008a) to separate source, path and site effects from the far-field *S*-wave Fourier spectra in three different tectonic regions of France (Pyrenees, Alps and Rhine Graben). The inversion is performed using acceleration spectra instead of the displacement spectra from the original method, and higher frequencies are now included (30 Hz instead of 15 Hz). All the spectra are corrected for crustal amplification so that the reference site is a generic rock site with $v_{s30} = 2000$ m s^{-1}. The κ values are computed by regression of the high-frequency part ($f \geq 10$ Hz) of the transfer functions.

The moment magnitudes resulting from our analysis show a good agreement, throughout the whole magnitude range, with the available moment magnitudes determined by the ETH Zürich. Our inverted moment magnitudes are linearly correlated to the local magnitude of French seismological agencies. In the range 2.5–5.5, local magnitude values are higher than our moment magnitude determinations. This discrepancy increases with the size of earthquakes. This point has already been observed in Deichmann (2006), Drouet *et al.* (2008a) and Edwards *et al.* (2008). We finally provide the first complete and homogeneous catalogue of moment magnitudes for France, for the events with magnitude greater than 3 that occurred between 1996 and 2006. Propagation and site terms determined in this study can also be used to estimate the moment magnitudes of any new event.

We observe an increase with magnitude for both Brune's stress drop and the apparent stress. Such increase has already been proposed by Mayeda & Walter (1996) and Kanamori & Rivera (2004) ($\Delta\sigma \propto M^{0.25}$). Resulting stress drops are lower in the Alps than in the other two regions (Pyrenees and Rhine Graben). This regional

variation could be explained by differences in the style of faulting. Events in the French Alps are located in a region with pre-dominant normal focal mechanisms (Sue *et al.* 1999; Kastrup *et al.* 2004). Events in the Pyrenees and Rhine Graben are usually characterized by strike-slip or reverse focal mechanisms (Eva *et al.* 1998; Rigo *et al.* 2005).

Our results show a regional dependence of the attenuation (for both geometric and anelastic attenuation). The Alps area is characterized by higher attenuation than the Rhine Graben or the Pyrenees areas, a conclusion also reached by Bakun & Scotti (2006) from their analysis of intensity data. However, large variations in the absolute value of Q lead to similar amplitude decays with distance (see the different models in Fig. 5). More data are then needed to constrain accurate values of Q.

The local site transfer functions have been determined and κ-values have been derived for each station. These κ determinations are based on the spectral high-frequency regression of the site transfer functions. An original method to determine v_{s30} for the rock stations is also proposed; comparing the resulting transfer functions with ratios of generic site amplifications allows us to estimate v_{s30}.

From this analysis, we then provide a v_{s30} range for the rock stations of the French accelerometric network (see Table 6). Our individual v_{s30}–κ estimates are compared with the Californian relationship developed by Silva *et al.* (1998). At first glance, the results suggest a correlation between v_{s30} and κ. However, considering the large uncertainties in both v_{s30} and κ estimates, the correlation becomes less clear. Additionally, Campbell (2009) showed that κ is strongly dependent on the thickness of the sedimentary layers for soft sites. This study provides a methodology to rapidly and easily estimate v_{s30} and κ for any rock station. Such data are needed to further test any correlation between v_{s30} and κ and understand the physical origin of κ at rock sites.

ACKNOWLEDGMENTS

The authors would like to warmly thank all the participants to the RAP program who were providing really high quality data. This work has been partly supported by the European Commission through the following projects: FP7-ENVIRONMENT-226967 entitled 'Seismic Hazard Harmonization in Europe'; and FP7-PEOPLE-248182 entitled 'Ground-motion modelling for seismic hazard assessment in regions with moderate-to-low seismic activity'. The authors thank David Halliday (GJI editor), John Douglas and Luca Malagnini (GJI reviewers) for their critical reviews and encouraging comments, which greatly helped to improve the manuscript as well as Sylvia Hales (GJI Editorial Assistant) for her helpful assistance. The authors are also grateful to François Thouvenot, Emmanuel Chaljub and Mathieu Causse for their careful internal reviews of this manuscript, as well as to Chris Van Houtte for his thorough check of the grammar and spelling of the text.

REFERENCES

Abercrombie, R.E., 1995. Earthquake source scaling relationships from −1 to 5 M_L using seismograms recorded at 2.5 km depth, *J. geophys. Res.,* **100,** 24 015–24 036.

Aki, K. & Richards, P.G., 2002. *Quantitative Seismology*, 2nd edn, University Science Books, Sausalito, California, 700 pp.

Akinci, A., Malagnini, L., Hermann, R.B., Gok, R. & Srensen, M.B., 2006. Ground motion scaling in the Marmara region, Turkey, *Geophys. J. Int.,* **166,** 635–651.

Anderson, J.G. & Hough, S.E., 1984. A model for the shape of the fourier amplitude spectrum of acceleration at high frequencies, *Bull. seism. Soc. Am.,* **74**(5), 1969–1993.

Andrews, D.J., 1986. Objective determination of source parameters and similarity of earthquakes of different size, in *Earthquake Source Mechanics*, pp. 259–267, eds Das, S., Boatwright, J. & Scholz, C.H., American Geophysical Monograph 37.

Atkinson, G.M. & Morrison, M., 2009. Observations on regional variability in ground-motion amplitudes for small-to-moderate earthquakes in North America, *Bull. seism. Soc. Am.,* **99**(4), 2393–2409.

Bakun, W.H. & Scotti, O., 2006. Regional intensity attenuation models for France and the estimation of magnitude and location of historical events, *Geophys. J. Int.,* **164,** 596–610.

Bay, F., Fäh, D., Malagnini, L. & Giardini, D., 2003. Spectral shear-wave ground-motion scaling in Switzerland, *Bull. seism. Soc. Am.,* **93**(1), 414–429.

Bay, F., Wiemer, S., Fäh, D. & Giardini, D., 2005. Predictive ground motion scaling in Switzerland: best estimates and uncertainties, *J. Seismol*, **9,** 223–240.

Bindi, D. *et al.*, 2009. Site amplifications observed in the Gubbio Basin, Central Italy: hints for lateral propagation effects, *Bull. seism. Soc. Am.,* **99**(2A), 741–760.

Bonilla, L.F., Steidl, J.H., Lindley, G.T., Tumarkin, A.G. & Archuleta, R.J., 1997. Site amplification in the San Fernando Valley, California: variability of site-effect estimation using the S-wave, coda and H/V methods, *Bull. seism. Soc. Am.,* **87**(3), 710–730.

Boore, D.M., 2003. Simulation of ground motion using the stochastic method, *Pure appl. Geophys.,* **160,** 635–676.

Boore, D. & Boatwright, J., 1984. Average body-wave radiation coefficients, *Bull. seism. Soc. Am.,* **74**(5), 1615–1621.

Boore, D.M. & Joyner, W.B., 1997. Site amplifications for generic rock sites, *Bull. seism. Soc. Am.,* **87**(2), 327–341.

Braunmiller, J., Deichmann, N., Giardini, D., Wiemer, S. & the SED Magnitude Working Group, 2005. Homogeneous moment-magnitude calibration in Switzerland, *Bull. seism. Soc. Am.,* **95**(1), doi:10.1785/0120030245.

Brune, J.N., 1970. Tectonic stress and the spectra of seismic shear waves from earthquakes, *J. geophys. Res.,* **75**(26), 4997–5009.

Brune, J.N., 1971. Correction, *J. geophys. Res.,* **76**(20), 5002.

Campbell, K.W., 2003. Prediction of strong ground motion using the hybrid empirical method and its use in the development of ground-motion (attenuation) relations in eastern North America, *Bull. seism. Soc. Am.,* **93,** 1012–1033.

Campbell, K.W., 2009. Estimates of shear-wave Q and κ_0 for unconsolidated and semiconsolidated sediments in Eastern North America, *Bull. seism. Soc. Am.,* **99**(4), 2365–2392.

Campbell, K.W. & Bozorgnia, Y., 2004. Erratum, *Bull. seism. Soc. Am.,* **94**(6), 2417.

Campbell, K.W. & Bozorgnia, Y., 2006. Next Generation Attenuation (NGA) empirical ground motion models: can they be used in Europe? *1st European Conference on Earthquake Engineering and Seismology*, 3–8 September 2006, Geneva, Switzerland, paper no. 458.

Campillo, M. & Plantet, J.-L., 1991. Frequency dependence and spatial distribution of seismic attenuation in France: experimental results and possible interpretations, *Phys. Earth planet. Inter.,* **67,** 48–64.

Chandler, A.M., Lam, N.T.K. & Tsang, H.H., 2006. Near-surface attenuation modelling based on rock shear-wave velocity profile, *Soil Dyn. Earthq. Eng.,* **26,** 1004–1014.

Cotton, F., Scherbaum, F., Bommer, J.J. & Bungum, H., 2006. Criteria for selecting and adjusting ground-motion models for specific target regions: application to Central Europe and rock sites, *J. Seismol*, **10**(2), doi:10.1007/s10950–005–9006–7.

Cotton, F., Pousse, G., Bonilla, F. & Scherbaum, F., 2008. On the discrepancy of recent European ground-motion observations and predictions from empirical models: analysis of KIK-net accelerometric data and point-sources stochastic simulations, *Bull. seism. Soc. Am.,* **98**(5), 2244–2261.

Deichmann, N., 2006. Local magnitude, a moment revisited, *Bull. seism. Soc. Am.,* **96**(4A), doi:10.1785/0120050115.

Douglas, J., 2003. Earthquake ground motion estimation using strong-motion records: a review of equations for the estimation of peak ground acceleration and response spectral ordinates, *Earth-Sci. Rev.,* **61,** 43–104.

Douglas, J., 2007. On the regional dependence of earthquake response spectra, *ISET J Earthq Technol*, **44**(1), 71–99.

Douglas, J., Gehl, P., Bonilla, L.F. & Gelis, C., 2010. A kappa model for mainland France, *Pure appl. Geophys.,* doi:10.1007/s00024-010-0146-5.

Drouet, S., Souriau, A. & Cotton, F., 2005. Attenuation, seismic moment, and site effects for weak-motion events: application to the Pyrenees, *Bull. seism. Soc. Am.,* **95**(5), 1731–1748.

Drouet, S., Chevrot, S., Cotton, F. & Souriau, A., 2008a. Simultaneous inversion of source spectra, attenuation parameters, and site responses: application to the data of the French accelerometric network, *Bull. seism. Soc. Am.,* **98**(1), doi:10.1785/0120060215.

Drouet, S., Triantafyllidis, P., Savvaidis, A. & Theodulidis, N., 2008b. Comparison of site effects estimation methods using the Lefkas (Greece) 2003 earthquake aftershocks, *Bull. seism. Soc. Am.,* **98**(5), 2349–2363.

Dubos, N., 2003. Contribution à l'évaluation du risque sismique dans les Pyrénées centrales, *Thèse*, Université Paul Sabatier, Toulouse III, France.

Dufumier, H., 2002. Synthesis of magnitude and focal mechanism computations for the $M \geq 4.5$ earthquakes in France for the period 1995-2000, *J. Seismol*, **6,** 163–181.

Edwards, B., Rietbrock, A., Bommer, J.J. & Baptie, B., 2008. The acquisition of source, path, and site effects from microearthquake recordings using Q tomography: application to the United Kingdom, *Bull. seism. Soc. Am.,* **98**(4), doi:10.1785/0120070127.

Eva, C., Pastore, S. & Deichmann, N., 1998. Evidence for ongoing extensional deformation in the western Swiss Alps and thrust-faulting in the southwestern Alpine foreland, *J. Geodyn*, **26**(1), 27–43.

Field, E.H. & Jacob, K.H., 1995. A comparison and test of various site-response estimation techniques, including three that are not reference-site dependent, *Bull. seism. Soc. Am.,* **85**(4), 1127–1143.

Frankel, A., 1991. Mechanisms of seismic attenuation in the crust: scattering and anelasticity in New York State, South Africa, and southern California, *J. geophys. Res.,* **96**(B4), 6269–6289.

Gagnepain-Beyneix, J., 1987. Evidence of spatial variations of attenuation in the western Pyrenean range, *Geophys. J. R. astr. Soc.,* **89,** 681–704.

Hanks, T.C., 1982. $f_{\max}$, *Bull. seism. Soc. Am.,* **72**(6), 1867–1879.

Hanks, T.C. & Kanamori, H., 1979. A moment magnitude scale, *J. geophys. Res.,* **84**(B5), 2348–2350.

Ide, S. & Beroza, G.C., 2001. Does apparent stress vary with earthquake size? *Geophys. Res. Lett.,* **28**(17), 3349–3352.

Kanamori, H. & Rivera, L., 2004. Static and dynamic scaling relations for earthquakes and their implications for rupture speed and stress drop, *Bull. seism. Soc. Am.,* **94**(1), 314–319.

Kastrup, U., Zoback, M.L., Deichmann, N., Evans, K.F., Giardini, D. & Michael, A.J., 2004. Stress field variations in the Swiss Alps and the northern Alpine foreland derived from inversion of fault plane solutions, *J. geophys. Res.,* **109,** B01402, doi:10.1029/2003JB002550.

Konno, K. & Ohmachi, T., 1998. Ground-motion characteristics estimated from spectral ratio between horizontal and vertical components of microtremor, *Bull. seism. Soc. Am.,* **88**(1), 228–241.

Malagnini, L., Mayeda, K., Uhrhammer, R., Akinci, A. & Hermann, R.B., 2007. A regional ground-motion excitation/attenuation model for the San Fransisco region, *Bull. seism. Soc. Am.,* **97**(3), 843–862.

Mayeda, K. & Walter, W.R., 1996. Moment, energy, stress drop, and source spectra of western United States earthquakes from regional coda envelopes, *J. geophys. Res.,* **101**(B5), 11 195–11 208.

Modiano, T. & Hatzfeld, D., 1982. Experimental study of the spectral content for shallow earthquakes, *Bull. seism. Soc. Am.,* **72**(5), 1739–1758.

Nicolas, M., Massinon, B., Mechler, P. & Bouchon, M., 1982. Attenuation of regional phases in western Europe, *Bull. seism. Soc. Am.,* **72**(6), 2089–2106.

Papageorgiou, A.S. & Aki, K., 1983. A specific barrier model for the quantitative description of inhomogeneous faulting and the prediction of strong ground motion, *Bull. seism. Soc. Am.,* **73**(4), 693–722.

Parolai, S. & Bindi, D., 2004. Influence of soil-layer properties on k evaluation, *Bull. seism. Soc. Am.,* **94**(1), 349–356.

Pequegnat, C., Guéguen, P., Hatzfeld, D. & Langlais, M., 2008. The French Accelerometric Network (RAP) and National Data Center (RAP-NDC), *Seismol. Res. Lett.,* **79**(1), 79–89.

Purvance, M.D. & Anderson, J.G., 2003. A comprehensive study of the observed spectral decay in strong-ground accelerations recorded in Guerrero, Mexico, *Bull. seism. Soc. Am.,* **93**(2), 600–611.

Rigo, A., Souriau, A., Dubos, N., Sylvander, M. & Ponsolles, C., 2005. Analysis of the seismicity in the central part of the Pyrenees (France), and tectonic implications, *J. Seismol*, **9**(2), 41–50.

Scherbaum, F., Cotton, F. & Smit, P., 2004. On the use of response spectral-reference data for the selection and ranking of ground-motion models for seismic-hazard analysis in regions of moderate seismicity: the case of rock motion, *Bull. seism. Soc. Am.,* **94**(6), 2164–2185.

Silva, W., Darragh, R., Gregor, N., Martin, G., Abrahamson, N. & Kircher, C., 1998. Reassessment of site coefficients and near-fault factors for building code provisions, Technical Report Program Element II: 98-HQ-GR-1010, Pacific Engineering and Analysis, El Cerrito, USA.

Stafford, P.J., Strasser, F.O. & Bommer, J.J., 2008. An evaluation of the applicability of the NGA models to ground-motion prediction in the Euro-Mediterranean region, *Bull. Earthq. Eng.,* **6,** 149–177.

Sue, C., Thouvenot, F. & Fréchet, J., 1999. Widespread extension in the core of the western Alps revealed by earthquake analysis, *J. geophys. Res.,* **104**(B11), 25 611–25 622.

Tarantola, A., 2004. *Inverse Problem Theory and Methods for Model Parameters Estimation*, SIAM, Philadelphia.

Thouvenot, F., 1983. Frequency dependence of the quality factor in the upper crust: a deep seismic sounding approach, *Geophys. J. R. astr. Soc.,* **73,** 427–447.